

Chapter 2

Materials

Abstract Structural materials must be able to operate under demanding exposure conditions. For advanced nuclear plants these are temperature, radiation and corrosive media. In principle there is no specific class of nuclear materials and the materials under discussion are the same as the ones used also for other applications. In this chapter the classification of the materials will be made according to their resistance to elevated and high temperatures. Specific nuclear aspects will only be briefly considered here. Nuclear and corrosion aspects are covered in [Chaps. 5 and 6](#). Starting with carbon steels and low alloy steels ferritic-martensitic steels, austenites and superalloys will be introduced. Intermetallics and nano-featured alloys with different matrices are considered as candidates for advanced applications. For very high temperatures and for some core internals and linings also ceramics are introduced.

2.1 Introduction

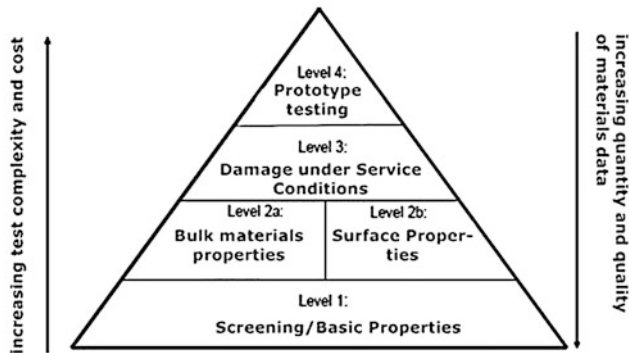
Structural materials are often limiting obstacles for technical progress of large machines. Reasons can either be missing properties (e.g. toughness, strength, creep strength, corrosion resistance etc.), missing production technologies, missing forming/joining techniques, or most important, high costs. For the current generation of nuclear light water reactors the structural materials have been well developed over the last 50 years. For them the long-time performance under service conditions (embrittlement, corrosion, fatigue) is of central interest. However, operational conditions for advanced new types of nuclear plants like the six generation IV reactors or fusion can no longer be accommodated only with materials currently used in nuclear power plants. The demands for structural materials increase because of more challenging exposure conditions (temperature, dose, environment). Established metallic materials can be used for long-time (about 100,000 h) in structural applications at temperatures up to about 950 °C.

For higher temperatures, higher loads and longer exposure times a change to other types of materials (ceramics) or significant improvements of metallic systems (oxide dispersion strengthening, refractory metals, intermetallics) are required. A major obstacle for the introduction of new materials for structural applications are the different time frames of materials research and development and the need of well established design data and component production routes necessary to build new types of plants even on a prototype basis. Some non-nuclear examples should highlight these problems: The use of ceramics or intermetallics in gas turbines has been discussed since very many years but due to toughness problems such concepts remained always in the experimental stage. Oxide dispersion strengthened materials, claimed in the eighties of the last century to provide a real step-forward in terms of allowable material temperatures never managed a break through because they could not be formed, reliably joined and they were too expensive. Supercritical steam turbines or coal gasification plants remained for long time at temperatures below 620 °C which was the maximum temperature which could be achieved with martensitic 9–12 % chromium steels. Higher temperatures would require nickel-base alloys which were considered for long time as being too expensive for these applications. But even for materials which could be successfully implemented the time from basic research to machine is typically 20–30 years as shown in Fig. 2.1.

The performance of materials used for current light water reactors is well established because also a 50 years operation experience exists which led to an ongoing improvement and optimization of the technical solutions. The introduction of new materials for nuclear applications suffers also from the stringent but necessary demands on safety and operational limitations. So called “rainbow-tests” where different prototypes of components or technical solutions are built into a machine to study its in-plant behavior for short time cannot easily be performed in a nuclear power plant. Additionally, any safety assessment, necessary for the approval of authorities, needs a technically sound basis which can only be provided in extended and expensive testing outside of the final application.

These different safety demands and the difficulty that changes have to undergo lengthy permit procedures are eventually one of the reasons why the communication between the nuclear materials society and the non-nuclear materials society is not as pronounced as it could be although the classes of materials used are more or less the same as shown in the following Table 2.1. From this table becomes clear that the materials considered for generation III+/IV reactors are basically the same as for most of advanced energy applications. The main differences are chemical environments and irradiation. Overcoming all these demands and limitations needs a thorough understanding of the materials and its properties which are based on elementary things like crystal structure, type and behavior of crystal defects etc. In the following the most important classes of structural materials for nuclear applications shall be introduced together with some basic materials properties.

Materials Design and Implementation



Level 1: 1-3 years

Level 2: 3-5 years

Level 3: 3-5 years

Level 4: 3-5 years (including prototype fabrication)

Total: 10- 15 years (assuming not sequential but parallel development work)

15-20+ years for nuclear materials

Fig. 2.1 The different steps of materials implementation, adapted from [1]

2.2 Basics

It is the aim of this section to introduce the most important features with respect to materials behaviour and materials damage. It is not considered to provide a thorough introduction into these subjects. For that we have to refer to the high number of excellent textbooks on physical metallurgy, materials science and crystallography like [3, 4]. This section here should help the reader who is not familiar with these topics to understand the reasons for materials degradation under conditions occurring in current and in advanced nuclear plants.

Structural materials consist of crystals which are based on regular arrangements of atoms in a crystal lattice. Metals and alloys are usually built up by many crystals which are called « grains ». The boundaries between grains are called « grain-boundaries » and the average size of grains is called « grain-size ». The basic behaviour of a crystal lattice is often studied with single crystals consisting of one grain only. Single crystals are of importance for the study of elementary properties. Technically, large and complex shaped components are difficult to be produced as single crystals. One exception are single crystalline nickel-base superalloys which are extremely temperature and stress resistant metallic materials. They are used as

Table 2.1 Classes of materials for advanced nuclear and advanced fossil power plants

Temperature		RT to 1,000 °C		RT to 1,200 °C	
Radiation Environments		0–300 dpa		0 dpa	
		Water, Steam, impure helium, liquid metals, molten salts		Gases (gasification, combustion), steam, water, low melting point eutectics, air	
Materials		Gen II + / Gen III + / Gen IV		Fusion Steam generators, heat exchangers, boilers (inkl. UHTC)	
		Gen II + / Gen III + / Gen IV		Steam turbines	
Low alloy steel		×	×	×	×
Ferritic/bainitic		–	×	×	×
Ferritic/martensitic		–	×	×	×
Austenitic		×	×	×	×
Duplex		–	–	×	–
<i>Superalloys</i>					
Solid solution		×	×	×	×
Gamma prime		×	×	–	×
Intermetallics		–	×	–	×
Nanostructured (ODS, gradient, bulk)		×	×	–	×
Refractory alloys		–	×	–	×
Ceramics (C, SiC, Oxides)		–	×	–	×
Coatings (corrosion, erosion, wear)		–	×	×	×

Only minor differences between nuclear and non-nuclear applications exist [2]

blades in gas-turbines and jet engines. Important materials properties are determined by crystal defects. It is discriminated between

- point defects (vacancies, interstitials)
- linear defects (dislocations)
- planar defects (stacking faults, antiphase boundaries)
- grain boundaries.

Point defects are of utmost importance for the understanding of irradiation damage and thermal properties. Movement of dislocations, glide planes, slip lines etc. describe plastic deformation and they are therefore a key to the understanding of irradiation induced changes in mechanical properties. Planar defects can be formed during deformation e.g. by cutting of particles and they are therefore also important for the understanding of mechanical properties. Grain boundaries are locations to which impurities can diffuse or where phases preferentially precipitate. They can be preferentially attacked by corrosive environment leading to corrosion damage.

Many properties, particularly of metals and alloys, depend on the chemical composition. Phase diagrams tell us what phases are formed depending on temperature and chemical composition. Although binary phase diagrams can only map a portion of the microstructure of a complex alloy they give important insight into it.

2.2.1 Point Defects

Figure 2.2 illustrates different types of point defects. Point defects occur when an atom is missing or when it is in an irregular place in the lattice structure.

Self interstitial atoms sit on inter-lattice sites and they occur usually only in low concentrations in metals because they distort and highly stress the lattice structure. They mostly occur in a form that two atoms share the same lattice site (Fig. 2.3). *Vacancies* are empty spaces where an atom is missing. They commonly occur, especially under irradiation conditions or at high temperatures when atoms frequently and randomly change their positions leaving behind empty lattice sites. Vacancy-interstitial pairs, so called « Frenkel Defects », are formed during irradiation with energetic particles like neutrons or ions. When an atom is displaced from its lattice site by the particle it occupies an inter-lattice position and a vacancy-interstitial pair remains as shown in Fig. 2.4. Vacancies and interstitials can annihilate, they can move to sinks or they can form clusters (vacancy cluster, interstitial cluster) which are particularly important for mechanical properties of irradiated materials (e.g. irradiation hardening). Further reactions of point defects created under irradiation will be discussed in Chap. 5.

An *interstitial impurity* is a small atom like e.g. hydrogen occupying an interstitial lattice position. An important example of interstitial impurity atoms are the carbon atoms in steels. Carbon atoms, with a radius of 0.071 nm, fit nicely in the open spaces between the larger (0.124 nm) iron atoms.

Fig. 2.2 Different point defects

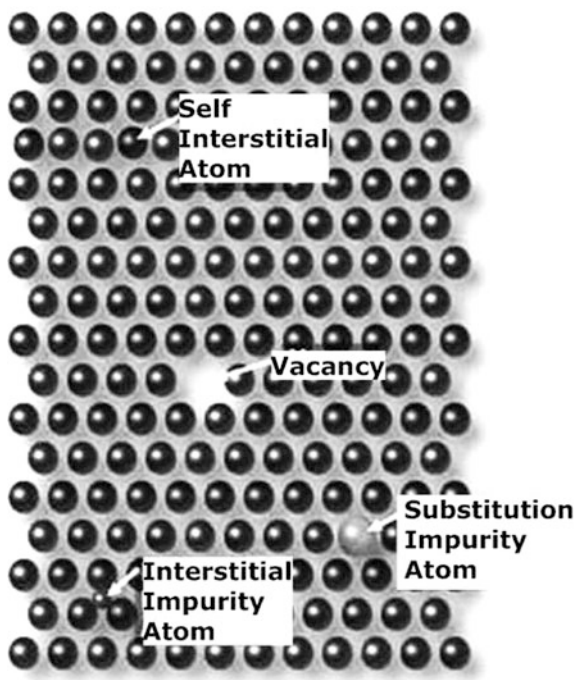


Fig. 2.3 Self-interstitial in body centered cubic lattice in dumbbell configuration. *Left side* regular lattice, *right side* lattice with interstitial

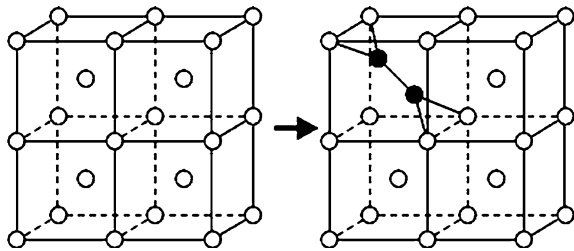
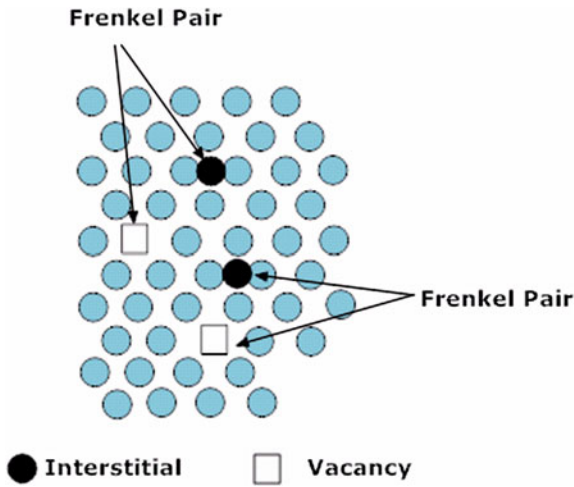


Fig. 2.4 Frenkel pair consisting of a vacancy-interstitial pair which are simultaneously created (e.g. by energy transfer from an energetic particle like a neutron)



A *substitutional impurity* atom is an atom of a different type than the bulk atoms, which has replaced one of the bulk atoms in the lattice. Substitutional impurity atoms are usually close in size (within approximately 15 %) to the bulk atom.

2.2.2 Linear Defects

Already in the first half of the last century it was found that:

- The stress required to plastically deform a crystal is much less than the stress one calculates from considering a defect-free crystal structure

and

- Deformation of a metal subsequent to a prior plastic deformation can require more stress for further plastic deformation (work hardening).

This led to the introduction of crystal defects explaining plastic deformation which were called “dislocations”. A missing half of a plane in a lattice creates a line-type defect around which the lattice is highly distorted. Such type of defect is called “edge dislocation”. The Burgers vector \mathbf{b} of a dislocation is a crystal vector, that quantifies the difference between the distorted lattice around the dislocation and the perfect lattice. It is therefore usually a lattice vector. There are two basic types of dislocations: The edge dislocation and the screw dislocation. The two types are shown in Fig. 2.5. The Burgers vector is perpendicular to the dislocation line for an edge dislocation and it is parallel to the dislocation line for a screw dislocation. Dislocations can move under an applied load in so called slip planes as shown in Fig. 2.5 and in more detail for an edge dislocation in Fig. 2.6. These Figures illustrate the action of dislocations as follows:

Reaching the final stage of a sheared crystal (Fig. 2.6 right) without a dislocation would require all atomic bonds in the glide-plane to be opened up at one time which needs a very high shear stress. Reaching the same sheared final stage of the crystal with a dislocation needs only opening the bonds adjacent to the dislocation line leading to movement of the dislocation. Under these circumstances a much lower shear stress is required for plastic deformation of the crystal.

Screw- and edge dislocations are the two basic types of dislocation lines. A dislocation line in a real lattice contains screw- and edge parts. Dislocations can also move from one glide-plane to a parallel one by cross slip (Fig. 2.7). The whole understanding of inelastic deformation (including creep), hardening and embrittlement is based on questions concerning the interactions of dislocations with existing or created obstacles. At elevated temperatures dislocations can climb over obstacles like particles when diffusion can happen. This will be discussed in more detail later.

The answer to the second question asked at the beginning of this subsection: i.e. why does deformation of a metal subsequent to a prior plastic deformation require more stress for further plastic deformation (work hardening) needs still to be

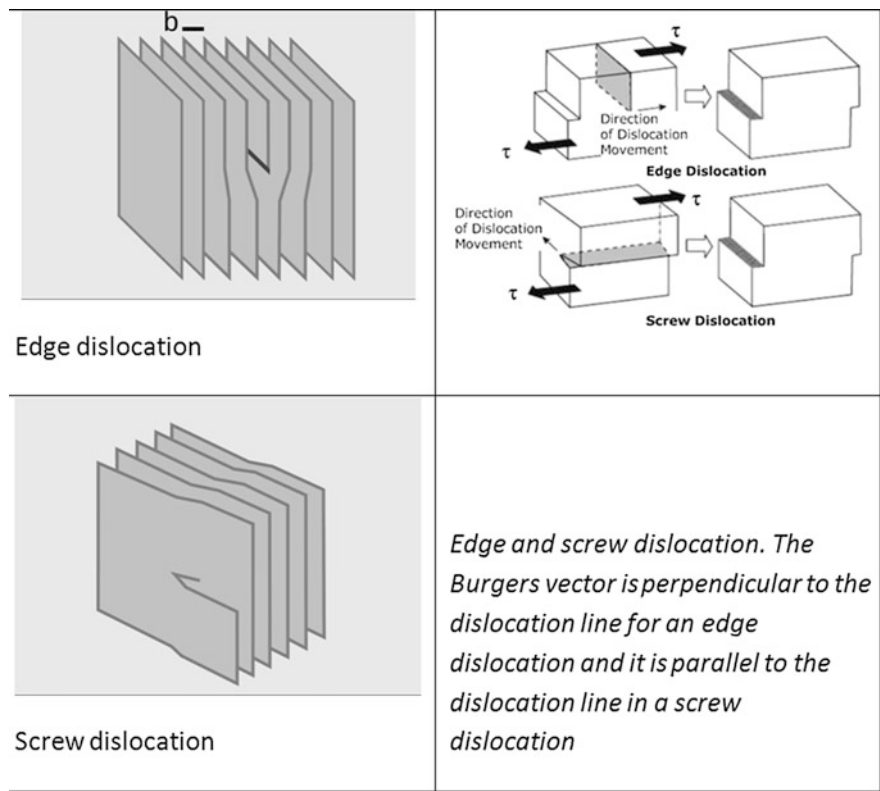


Fig. 2.5 Edge dislocation and screw dislocation and its movement through the crystal sources: <http://en.wikipedia.org/wiki/Dislocation> and [5]

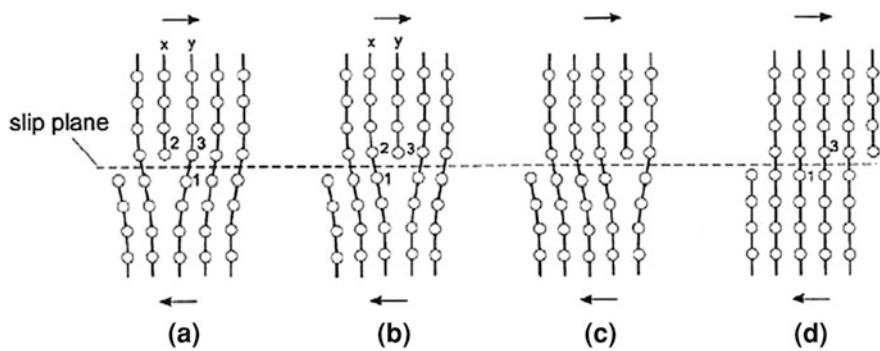


Fig. 2.6 Movement of an edge-dislocation through a crystal. Only the bonds adjacent to the dislocation must be broken up to shear the material. This means that the shear stress is lower than if several bonds in the glide plane had to be simultaneously broken. (source [5])

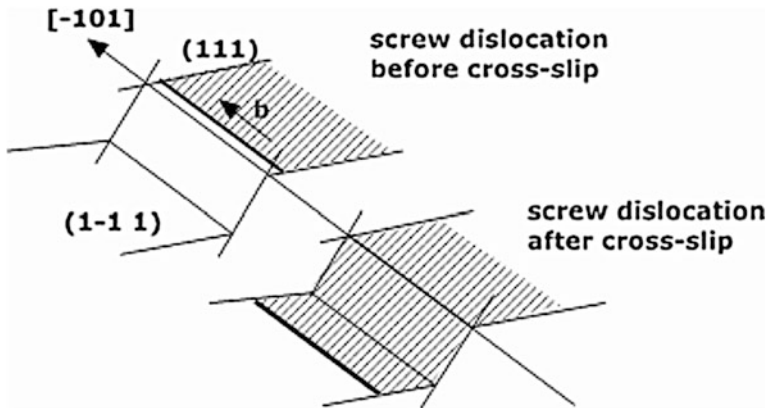


Fig. 2.7 Cross slip happens when an additional glide plane (cross-slip plane) can become active (after [5])

considered. Higher dislocation density increases yield strength and causes work hardening of metals. This requires an increase in dislocations density or dislocation multiplication. The Frank-Read Source [6] (Fig. 2.8) is a mechanism to explain this phenomenon. Consider a straight dislocation in a crystal slip plane with its two ends, A and B, pinned (Position 0). If a shear stress τ is exerted on the slip plane then a force is exerted on the dislocation line as a result of the shear stress. This force acts perpendicularly to the line, inducing the dislocation to lengthen and curve into an arc. If the shear stress increases any further and the dislocation passes the semicircular equilibrium state (Position 1), it will spontaneously continue to bend and grow, spiraling around the A and B pinning points (Position 2). The two adjacent segments of the highly bowed out dislocation touch each other. Since the two line vectors at the point of contact have opposite signs, the segments in contact will annihilate each other (Position 3). A dislocation loop and again a dislocation pinned at A and B will form (Position 0). The loop moves further through the crystal and interacts with other dislocations or grain boundaries. The newly formed line between A and B undergoes now the same process as just described and so on which leads to an increase of the dislocation density (Fig. 2.8).

2.2.3 Planar Defects

Planar defects are:

- stacking faults
- antiphase boundaries
- grain boundaries.

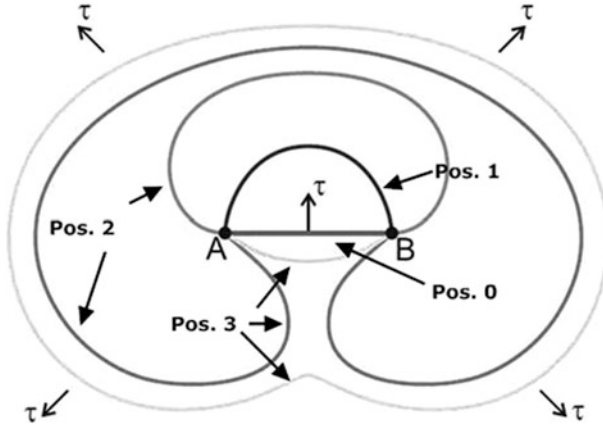


Fig. 2.8 Dislocation creation by a Frank-Read source. Under an acting shear stress τ the dislocation line AB starts to bow until a dislocation loop and again a dislocation line AB are formed. Further information is given in the text [6]

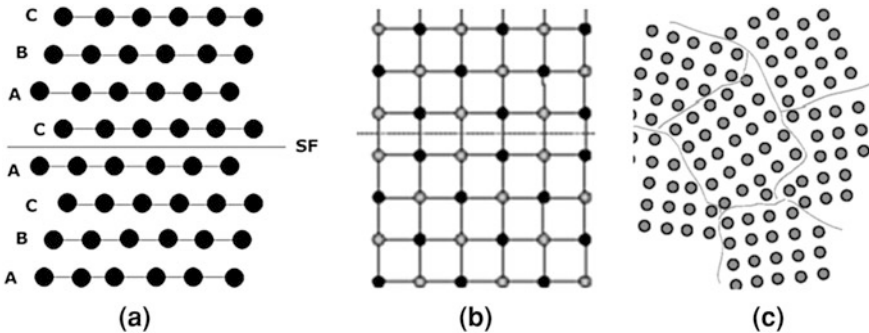


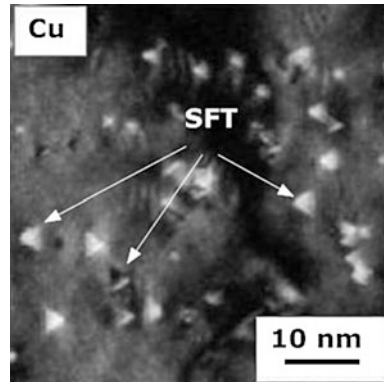
Fig. 2.9 Different types of planar defects. At a stacking fault the stacking sequence is disturbed. In an ordered lattice such a disturbance can create an antiphase boundary. Grain boundaries are the areas where different crystals grow together

They are shown as sketches in Fig. 2.9.

Stacking faults are formed when the stacking sequence of crystallographic planes is disturbed. Figure 2.9a shows a case in which the sequence CBAC-BACBA is changed to CBACACCBA. These interruptions of the stacking sequence carry a certain stacking fault energy. Reasons for the development of stacking faults can be the split of dislocations into partial dislocations [7] or formation of dislocations loops.

Besides planar stacking faults also (3-dimensional) stacking fault tetrahedra exist. They can also be created by irradiation (see e.g. [8] and Fig. 2.10). Stacking fault tetrahedra are at a first glance a peculiar shape of defects, but they are a more common type of vacancy clustered defects than simple planar shape dislocation

Fig. 2.10 Irradiation induced stacking fault tetrahedra in copper irradiated at room temperature at a dose of 0.046 dpa (replotted from [8])



loops (see e.g. [9] for more details). Such tetrahedra can interact with dislocations leading to an increase in yield stress which will be discussed in another section.

The antiphase boundary (Fig. 2.9b) has similarities with the stacking fault. It can be considered as some stacking fault in an ordered crystal layer like an intermetallic phase. In such a case a change in stacking sequence means also a change in the periodic arrangement of the different atoms. The micrograph shown in Fig. 2.11 shows planar defects in a γ' hardening nickelbase superalloy. Particles are cut by dislocations creating antiphase boundaries and stacking faults which are visible as fringe contrast in the micrograph.

Agglomeration of point defects leads to dislocation loops (Fig. 2.12). Dislocation loops as shown in Fig. 2.12 are formed by agglomeration of interstitials leading to an interstitial type of loops whereas an agglomeration of vacancies leads to a vacancy type of loop. Loops are surrounded by dislocations with certain Burgers vector. The plane of the loop is called habit plane. Dislocation loops can impede the movement of dislocations leading to hardening and consequently often to embrittlement. Figure 2.13 shows two transmission electron micrographs of dislocation loops in an oxide dispersion strengthened ferritic steel after helium implantation.

Grain boundaries which are the border between the crystals (Fig. 2.9c) are also classified as planar defects. They play a very important role with respect to materials degradation and also with respect to irradiation damage as we will see later.

2.2.4 Diffusion Processes

Processes in solids are governed by laws of thermodynamics and kinetics. Thermodynamics tells if a process can occur and what is the driving force behind it. The laws of kinetics describe how quickly reactions or processes happen. Gibbs energy (also referred to as G) is the chemical potential that is minimized when a system reaches equilibrium at constant pressure and temperature. The relation

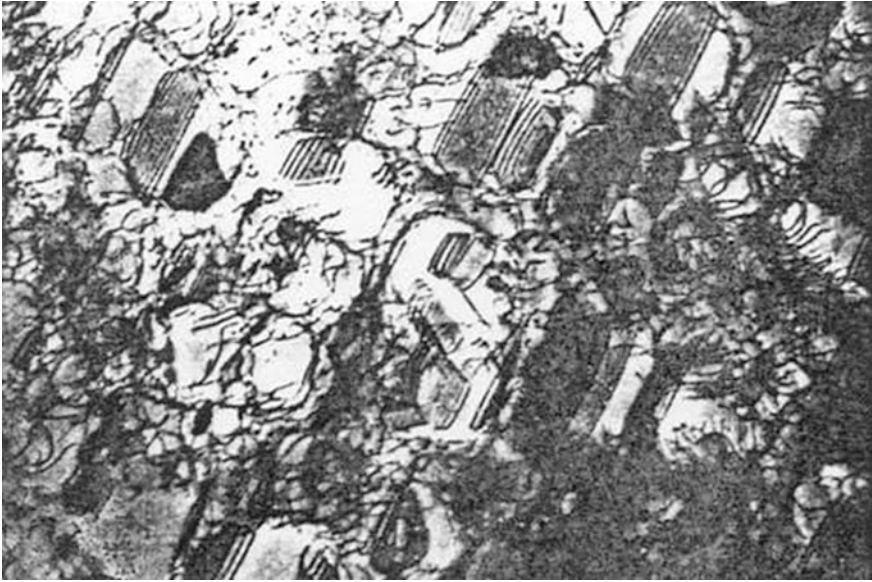
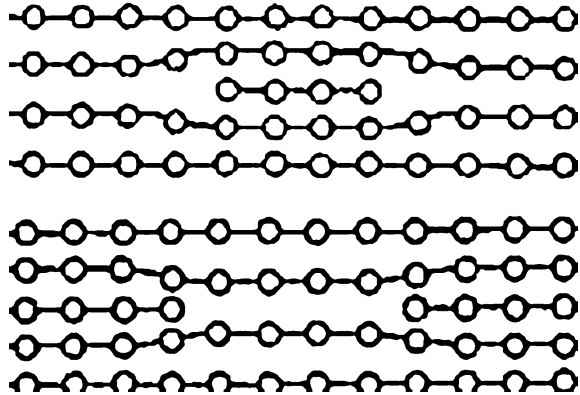


Fig. 2.11 Planar defects (antiphase-boundaries/stacking faults) in a nickel-base superalloy visible as fringe patterns in a TEM micrograph

Fig. 2.12 Dislocation loops interstitial type (a), vacancy type (b)



between the thermodynamic state variables Enthalpy H , Entropy S , Gibbs energy G and the temperature is given as

$$G = H - T.S \quad (2.1)$$

This relationship is important for phase diagrams introduced in the following section.

Let ΔG be the difference of G between two states which drives the reaction and ΔG_a the activation energy which must be overcome that the process can happen.

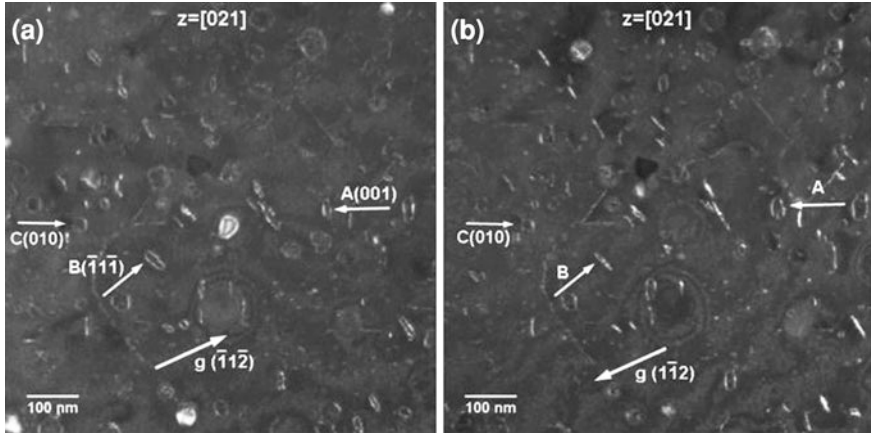


Fig. 2.13 Dislocation loops in an oxide dispersion strengthened ferritic steel after helium implantation

The reaction speed, r , giving the reacted mass per unit time can be written as a thermally activated process:

$$r \sim (\Delta G)^k \cdot e^{-\frac{\Delta G_a}{R.T}} \quad (2.2)$$

where:

$1 \leq k$

R Gas Constant

T Temperature (in K)

Relation 2.2 can be applied to atoms or mol leading to:

$$r = r_0 \cdot e^{-\frac{\Delta G_a^{(atom)}}{R.T}} \quad \text{or} \quad r = r_0 \cdot e^{-\frac{\Delta G_a^{(mol)}}{R.T}} \quad (2.3)$$

Atoms can move (diffuse) through the lattice provided that there is a space where they can move to and that the atoms have enough energy (activation energy) to break the bonds to move to this site. Increasing temperature or collisions of lattice atoms with energetic particles (radiation damage) increase the energy of atoms and therefore the probability to move to other lattice positions. Two main types of lattice diffusion can occur:

- Interstitial diffusion (Fig. 2.14)
- Substitutional diffusion (Fig. 2.15)

In a metal the interstitial atoms can either be identical with the base metal (self interstitials) or they can be small impurity atoms like: hydrogen, oxygen, nitrogen, carbon, boron, sulphur. Interstitial diffusion can easily occur because the atom has to move only to the next free interstitial site. As usually the interstitial atoms occur with low density only the probability that a next interstitial site is already occupied is very

Fig. 2.14 Movement of an interstitial atom through the lattice (*top*) and schematic of the free activation enthalpy of the jump (*bottom*)

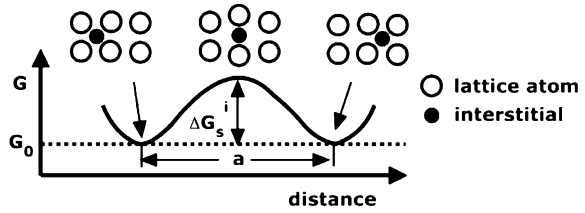
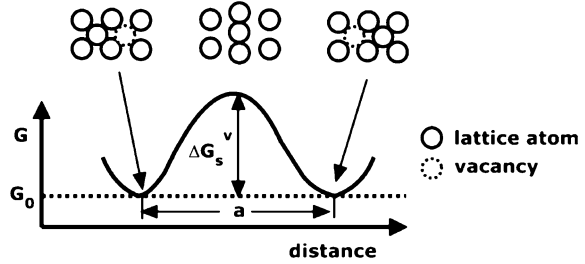


Fig. 2.15 Movement of a regular atom through the lattice (*top*) and schematic of the free activation enthalpy of the jump (*bottom*)



low. Regular diffusion needs movement of vacancies. Also this type of diffusion can happen with base-metal atoms (lattice self diffusion) or with foreign atoms.

Diffusion is mainly governed by the jumping frequency of atoms. In case of interstitial diffusion which needs only a vacant interstitial site to occur the jumping frequency Γ_i is related to the temperature according to Eq. (2.4)

$$\Gamma_i \sim e^{\frac{-\Delta G_i^a}{R.T}} \quad (2.4)$$

with ΔG_s^a activation enthalpy/mol of a jump.

Lattice diffusion can only happen when a vacancy adjacent to the atom is available. The jumping frequency is

$$\Gamma_i \sim x_v e^{\frac{-\Delta G_s^a}{R.T}} \quad (2.5)$$

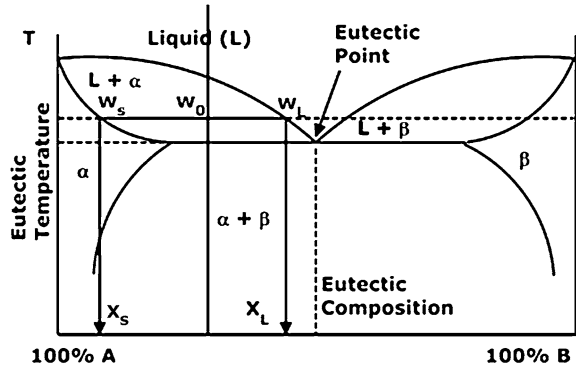
with x_v equilibrium concentration of vacancies.

The jumping frequency increases when a high number of point defects (as during irradiation with energetic particles) is present which will be discussed in the irradiation damage section more in detail.

The movement of atoms through the lattice is equivalent to the transport of matter. When two solid phases are in contact and the temperature is high enough the mass transport can lead to a volume increase of one phase and consequently to a volume decrease of the other phase. This so called Kirkendall effect [10] which describes matter transport in solids due to diffusion is an experimental proof for the occurrence of matter diffusion.

But also diffusion of point defects to sinks leads to mass transport. This phenomenon which plays an important role for irradiation induced materials transport like radiation induced segregation is called inverse Kirkendall effect it will also be discussed in the irradiation damage section.

Fig. 2.16 Typical binary phase diagram



The flux J (atoms/[unit area . time] or mass/[unit area . time]) of one of the components, at a given time, and any point along the profile, may be written as:

$$J = -D \frac{\partial c}{\partial x} \quad (2.6)$$

where c is the concentration D is a constant known as the *diffusivity* or the *diffusion coefficient* (length²/time). This differential equation is referred to as Fick's First Law.

The evolution of concentration with both time and distance along the couple is described by Fick's Second Law:

$$\frac{\partial c}{\partial t} = - \frac{\partial J}{\partial x} = D \frac{\partial^2 c}{\partial x^2} \quad (2.7)$$

where the concentration is expressed as a function of distance and time, $c(x, t)$. Diffusion can be influenced by lattice defects like dislocations or grain boundaries. Dislocations are linear defects and diffusion is enhanced along the core of a dislocations (pipe diffusion). Diffusion is also enhanced along grain boundaries (grain boundary diffusion) which is an important process for thermal creep as discussed in [Chap. 4](#).

2.2.5 Binary Phase Diagrams

The phase diagram shows the equilibrium states of a mixture. It allows to determine which phases will be formed at a certain temperature and composition. The main theory behind phase diagrams is based around the latent heat that is evolved when a mixture is cooled, and changes phase. This means that by plotting graphs of temperature against time for a variety of different compositions, it should be possible to see at what temperatures the different phases form. A schematic of a typical simple binary phase diagram is shown in [Fig. 2.16](#).

L stands for liquid, and A and B are the two components and α and β are two solid phases rich in A and B respectively. The liquidus lines represent the boundaries under which everything becomes liquid, whereas the solidus lines represent the boundaries under where the alloy is solid when cooling down from the melt. There are also lines for the solidified material along which phase transitions occur. A eutectic system is a mixture of chemical compounds or elements that has a single chemical composition that solidifies at a lower temperature than any other composition. This composition is known as the eutectic composition and the temperature is known as the eutectic temperature. Eutectic phases can also form in the solid state. They are called eutectoids.

It is also important to determine the amount of phases which is formed when cooling down. The *lever rule* is a tool used to determine weight percentages of each phase of a binary equilibrium phase diagram. As first step the “tie-line” for the temperature of interest must be drawn. This is a line parallel to the composition axis drawn at the temperature of interest. The percent weight of element B at the liquidus is given by w_l and the percent weight of element B at the solidus is given by w_s . The percent weight of solid and liquid can then be calculated using the following lever rule equations:

Percent weight of the solid phase, X_s :

$$X_s = \frac{w_0 - w_l}{w_s - w_l} \quad (2.8)$$

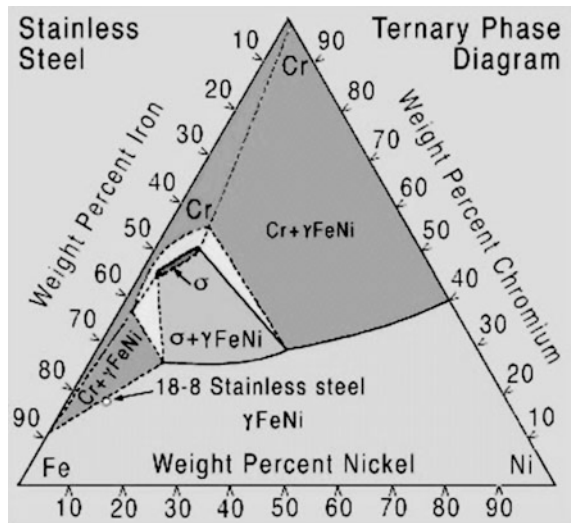
Percent weight of the liquid phase, X_l :

$$X_l = \frac{w_s - w_0}{w_s - w_l} \quad (2.9)$$

where w_0 is the percent weight of element B for the given composition. The lever rule remains also valid for determination of weight fractions of phases in the solid state. Alloys are usually mixtures of more than two elements. Phase diagrams can also be determined for three constituents (ternary phase diagram) as shown for an austenitic Fe–Ni–Cr steel (Fig. 2.17). They are usually drawn at certain temperatures. For a detailed introduction into phase diagrams we refer to the excellent web-textbook of the University Cambridge [12] or to other literature [13–15].

An essential point to remember is that both, the theory and the experiments to construct phase diagrams rely on the assumption that the system is in equilibrium, which is rarely the case, as this only occurs properly when the system is cooled very slowly. In order to reach full equilibrium, the solute in the solid phases must stay completely uniform throughout the cooling. However, in most systems, if the system is not cooled quickly, the phase diagram will give fairly accurate results. In addition, near the eutectic, the results become even closer to the phase diagram, as the liquid solidifies at nearly the same time. Segregations and phase formations in alloys after long-time exposure to elevated temperatures are a result of not reaching an equilibrium in the solid state at room temperature. The non equilibrium conditions can sometimes be of benefit however, as microstructures at higher

Fig. 2.17 Ternary Fe–Ni–Cr diagram at 900 °C (with permission of ASM [11])



temperatures in phase diagrams may sometimes be preserved to lower temperatures by fast cooling, i.e. quenching, or unstable microstructures may occur during fast cooling which can be useful when hardening an alloy.

2.3 Classes of Materials for Nuclear Applications

For structural nuclear applications basically the following classes of materials are considered:

- metals and alloys
- intermetallics
- ceramics (bulk and fiber reinforced)
- Layered structures

Steels, superalloys, oxide dispersion strengthened steels/superalloys, refractory alloys belong to the metals and alloys class, aluminides are important intermetallics, graphite, carbon, silicon carbide and oxides (like zirconia) are the main ceramics discussed. Several deposited layers to prevent corrosion attack are considered for advanced nuclear reactors like the lead cooled fast reactor, the supercritical water reactor or the molten salt reactor.

Current nuclear power plants employ mainly low alloy steels, austenitic steels and superalloys as structural parts and zirconium based alloys as fuel cladding. The main reason for this choice are the strength/toughness requirements for the pressure boundaries, good liquid corrosion resistance and neutronics. The demands coming from new nuclear plants need structural materials with better performance at higher temperatures and higher doses in environments different from water. Finally, or

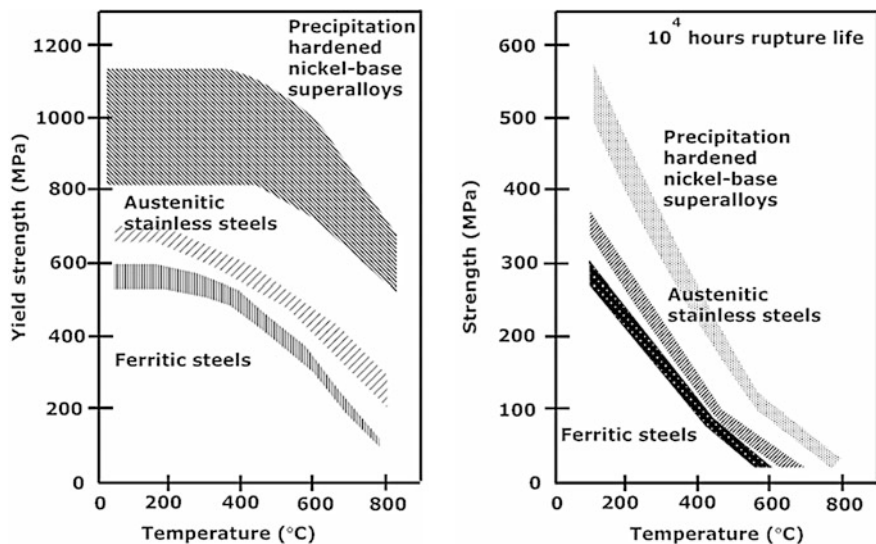


Fig. 2.18 Comparison of yield strengths and stress rupture properties of ferritic steels, austenitic steels and nickel based superalloy [16, 17]

even primarily all improvements have to be made at affordable costs. These very demanding requirements cannot be achieved with one specific material but several classes of materials tuned to the local conditions in the plant must be considered. However, it must be mentioned that nuclear materials development is not an isolated branch of materials research. Almost all materials which we will consider now are needed also in other, non-nuclear, energy related applications like gas-turbines, steam-turbines, boilers, coal-gasification plants or solar thermal plants.

The main driving forces for the development of structural materials for nuclear applications are radiation resistance (embrittlement and swelling) and the performance at elevated to high temperatures where time dependent effects become important. In this chapter the materials shall be developed according to its high temperature properties. Radiation induced limitations will mainly be discussed in the radiation damage section.

High temperature strength depends on the class of materials as illustrated with an example shown in Fig. 2.18. Two mechanical properties are primary of concern: yield strength and creep rupture strength (see Chap. 4). Yield strength and 10^4 h creep rupture strength (see also Chap. 4) are plotted as a function of temperature. It can be seen that systematically the high-temperature strength properties increase from ferritic steels through austenitic steels to nickel-based superalloys.

Possibilities to improve performance of structural materials for advanced (nuclear) applications are as follows:

- changing composition or matrix/base metal
- creating obstacles for dislocation movement by alloy composition (precipitates)

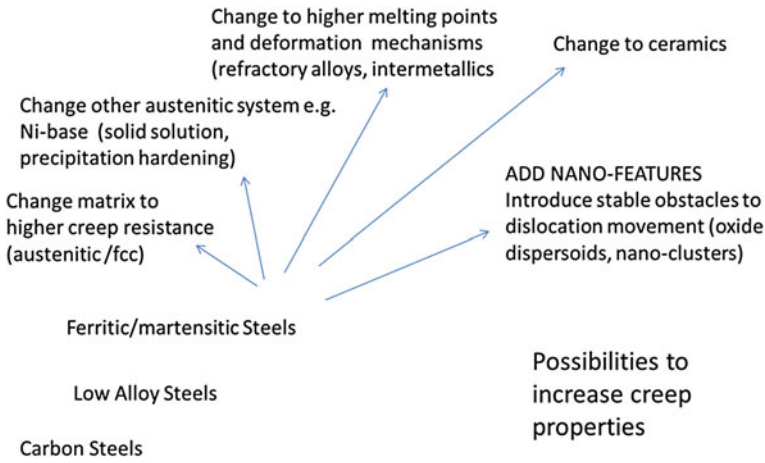
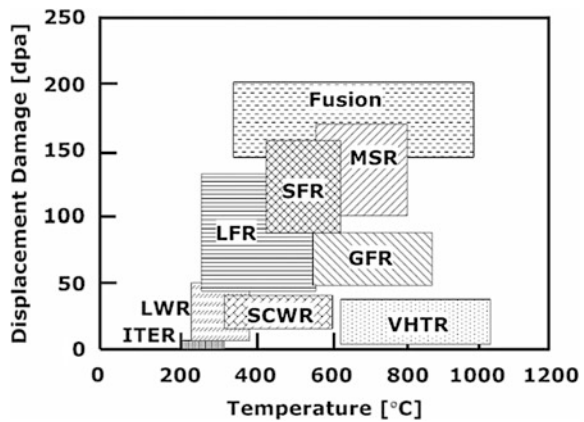


Fig. 2.19 Possibilities to increase high temperature strength of structural materials

Fig. 2.20 Expected radiation damage and operation temperatures of different advanced nuclear plants (source [18])



- introducing obstacles for dislocation movement from outside (dispersoids)
- changing from metallic systems to ceramic systems

Drawbacks like missing toughness, missing corrosion properties, missing forming/shaping or welding possibilities and high production costs are main reasons why the introduction of advanced materials proceeds very slowly and is sometimes even stopped. Figure 2.19 gives a schematic classification of the different classes of materials with respect to its high temperature performance. Besides good high temperature strength materials for advanced nuclear plants are also expected to have a high radiation resistance. Figure 2.20 compares the temperature and radiation damage conditions in different current and advanced nuclear technologies. The term displacement damage and the unit “dpa” are explained in Chap. 5. Often a discrepancy between good high temperature strength and irradiation resistance of

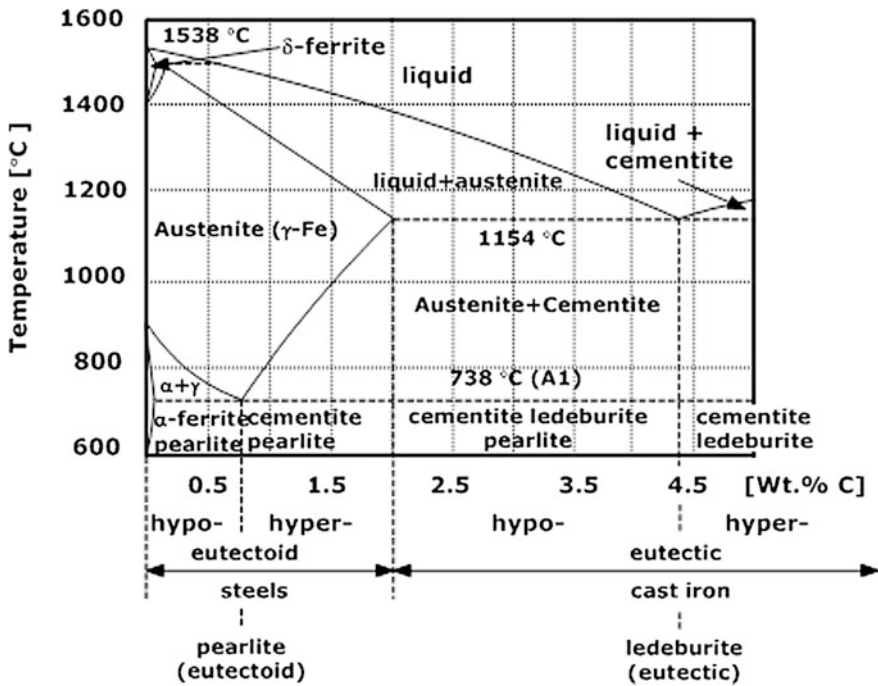


Fig. 2.21 Binary iron-carbon phase-diagram

materials exist. The current chapter will mainly deal with thermal properties of the different classes of materials as already mentioned. The scheme shown in Fig. 2.19 shall be further explored and the different classes of materials will be discussed. Production related aspects are deeper considered in Chap. 3.

2.3.1 Steels

Steels have been the most important structural materials since long time and they will remain the most important structural material also for advanced nuclear plants. The basis for steels is the iron-carbon phase diagram which is shown in Fig. 2.21. The specific properties of the different classes of steels are a result of the carbon content, alloying elements and heat treatment. The following short description follows the introduction given in the literature [19].

The steel portion of the metastable Fe-C phase diagram (0–2.08 wt. % C) can be subdivided into three regions:

- hypoeutectoid (0 < wt. % C < 0.68 wt. %)
- eutectoid (C = 0.68 wt. %)
- hypereutectoid (0.68 < wt. % C < 2.08 wt. %).

The cast iron portion of the Fe–C phase diagram covers the range between 2.08 and 6.67 wt. % C. Cooling down from the melting temperature of iron (1,538 °C) δ -ferrite, which is a solid solution of carbon in iron, is formed. The maximum concentration of carbon in δ -ferrite is 0.09 % (at 1493 °C). Its crystal structure is body centered cubic (bcc).

Cooling further down the following phases are obtained (from low carbon side to high carbon side):

- Austenite—which is an interstitial solid solution of carbon in γ -iron. Austenite has a face centered cubic crystal structure (fcc). In austenite the carbon concentration can reach up to 2.06 wt. % (at 1,147 °C).
- Liquid phase plus austenite
- Liquid phase plus cementite; cementite is an iron carbide with the formula Fe_3C . It has an orthorhombic crystal structure. It is a hard, brittle (ceramic) material.
- At 1,147 °C the eutectic point is reached where austenite and cementite are formed.

Below 738 °C austenite is no longer stable. At this temperature a eutectoid (solid–solid) is formed consisting of ferrite and cementite. At very low carbon contents (max. 0.025 wt. % at 738 °C) ferritic α -iron is obtained. The much larger phase field of gamma-iron (austenite) compared with that of alpha-iron (ferrite) indicates clearly the considerably greater solubility of carbon in gamma-iron (austenite), the maximum value being 2.08 wt. % at 1,154 °C. The iron-carbon binary system shows the following critical temperatures:

- Upper critical temperature (point) A_3 is the temperature, below which ferrite starts to form as a result of ejection from austenite in the hypo-eutectoid alloys.
- Upper critical temperature (point) A_{CM} is the temperature, below which cementite starts to form as a result of ejection from austenite in the hypereutectoid alloys.
- Lower critical temperature (point) A_1 is the temperature of the austenite-to-pearlite eutectoid transformation. Below this temperature austenite does not exist.
- Magnetic transformation temperature A_2 is the temperature below which α -ferrite is ferromagnetic

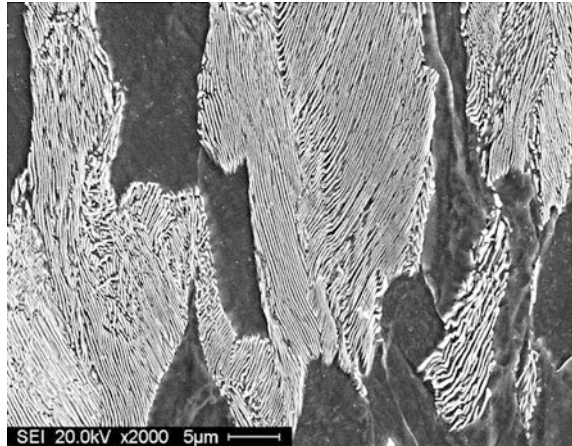
At room temperature the following phases are found additionally to α -iron: Cementite, pearlite and ledeburite

Ledeburite is the eutectic mixture of austenite and cementite. It contains 4.3 % Carbon and represents the eutectic of cast iron. Ledeburite exists when the carbon content is greater than 2 %, which represents the dividing line on the equilibrium diagram between steel and cast iron.

Pearlite is the eutectoid mixture containing 0.83 % Carbon and is formed at 727 °C on very slow cooling. It is very fine platelike or lamellar mixture of ferrite and cementite. The structure of pearlite (Fig. 2.22) shows the ferritic matrix which also includes thin plates of cementite (see also [26]).

In summary can be concluded that the vast majority of steels rely on just two allotropes of iron: (1) alpha-iron, which is body-centered cubic (bcc) ferrite, and

Fig. 2.22 Pearlitic structure
(source [20])



(2) gamma-iron, which is face-centered cubic (fcc) austenite. At ambient pressure, bcc ferrite is stable from all temperatures up to 912 °C (the A_3 point), when it transforms into FCC austenite.

It can be seen, that below about 740 °C no austenitic phase exists. At room temperature ferrite and iron carbide (cementite) are expected. This brief description of the iron-carbon phase diagram should be sufficient for the understanding of steels for nuclear applications. For a more detailed description of the iron-carbon diagram we have to refer to other literature or textbooks e.g. [21].

From the binary iron-carbon phase diagram it is not possible to get information about how austenitic steels or martensitic steels can be produced. This needs additional alloying elements and heat treatments.

The austenitic matrix can be stabilized at room temperature by adding alloying elements like chromium, nickel or molybdenum. A very important representation of the conditions under which austenite is stable is the “Schaeffler Diagram” [22] which is shown in Fig. 2.23. It shows the tendency for formation of austenite, ferrite, martensite and it’s mixtures as a function of chromium equivalent and nickel equivalent. The chromium equivalent is the sum of ferrite forming elements; nickel is an austenite former. The Schaeffler diagram is also very important with respect to weldments, to obtain the required microstructure in the area of the weld.

After this brief discussion of compositions under which austenite can be formed, we have to address the question of formation of martensite. For this purpose phase transformation diagrams have to be visited. There are two main types of transformation diagrams that are helpful in selecting the optimum steel and processing route to achieve a given set of properties. These are time–temperature transformation (TTT) and continuous cooling transformation (CCT) diagrams [24]. CCT diagrams are generally more appropriate for engineering applications as components are cooled (air cooled, furnace cooled, quenched etc.) from a processing temperature which is more economic than transferring them to a separate furnace for an isothermal treatment.

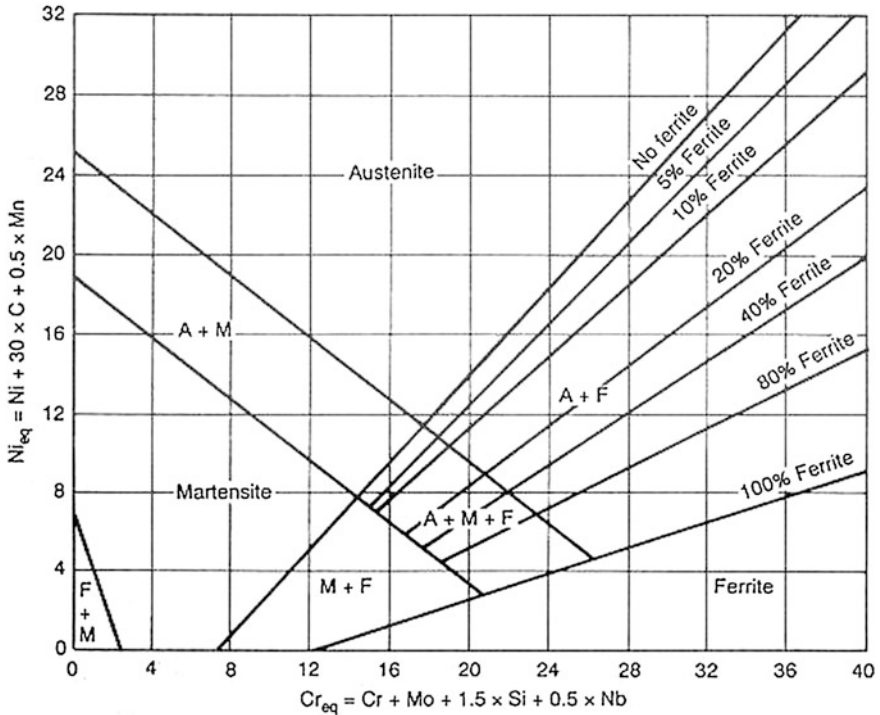


Fig. 2.23 Schaeffler Diagram (replotted from [23])

A time–temperature transformation (TTT) diagram is obtained when the steel is cooled down from the austenitization temperature to a lower temperature which is kept constant. The rate of transformation at this temperature can now be measured e.g. with a dilatometer. Such diagrams are important to determine what happens during thermal treatment.

In contrast to the TTT provides the continuous cooling transformation (CCT) the basis for determination of the extent of transformation as a function of time for a continuously decreasing temperature. In other words a sample is austenitized and then cooled at a predetermined rate and the degree of transformation is measured, for example by dilatometry. These results are important to determine the local microstructure of a component in dependence of local cooling rate (e.g. during quenching of large components).

Figure 2.24 shows a typical CCT-diagram for steel. The cooling line refers to intermediate cooling rate. Under the shown conditions the formation of a bainitic structure can be expected. Quenching down from the austenitization temperature leads to martensite, whereas slow down-cooling leads to ferritic/pearlitic microstructure. The CCT-diagram is very important for the assessment of microstructure developing during heat treatment of a component. Cooling rates at the surface of a component are faster than the ones in the center. This means that e.g. a martensitic

Fig. 2.24 Typical CCT-diagram for steel. An intermediate cooling rate leads to bainitic structure. Quenching would lead to martensite and slow cooling would lead to ferritic-pearlitic structure (after [24])

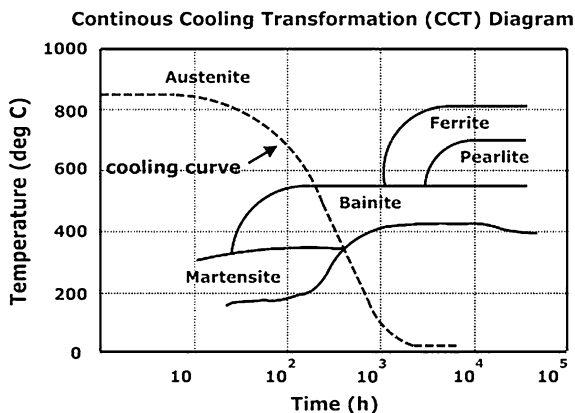


Table 2.2 Dependence of tensile data from location in the forging for a typical RPV steel; *t* designates the thickness of the forging

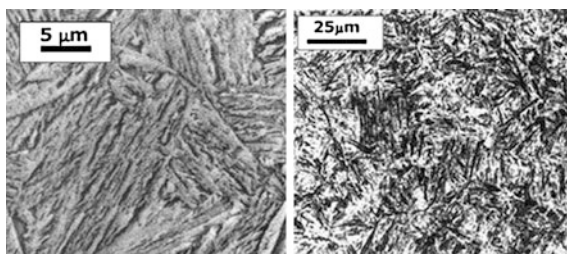
Location	Yield strength [MPa]	Tensile strength [MPa]	Elongation[%]	Reduction of area [%]
Top 0/4 <i>t</i>	564	688	26	82
Top 1/4 <i>t</i>	487	635	25	77
Top 2/4	482	630	24	77
Bottom 0/4 <i>t</i>	548	678	27	81
Bottom 1/4 <i>t</i>	467	624	27	76
Bottom 2/4 <i>t</i>	465	611	27	77

In the outer part (*top, bottom 0/4t*) the material is stronger as a result of faster cooling rates [25]

microstructure can develop at the surface whereas a bainitic-pearlitic structure develops in the center which also means that different mechanical properties exist in such a component. This can be illustrated with results from plates of a reference material for a reactor pressure vessel steel (JRQ) where almost 20 % higher yield stress was measured at the surface compared with the interior of the plate [25] as shown in Table 2.2.

Diagrams mapping the development of phases with time of thermal exposure are also often referred to as “time–temperature–phase” (TTP)—diagrams. The microstructure of pearlite has been shown already in Fig. 2.22. Microstructures of bainite and martensite are mainly governed by the response of the carbon atoms. If there is enough time for diffusion of carbon a pearlitic structure can be developed. If there is not enough time for diffusion cooling down happens without the loss of carbon atoms into cementite and ferrite. Instead, the carbon is retained in the iron crystal structure, which is stretched slightly so that it is no longer cubic. The face centered cubic lattice of austenite is distorted into the body centered tetragonal structure which is called martensite. During a subsequent heat treatment

Fig. 2.25 Different types of steel developing as a result of different cooling rates.
 (a) (lower)bainite (Source: [27]). (b) martensite (Source: [28])



(tempering) the distortion can be slightly released and also some carbides are precipitated (tempered martensite) (Fig. 2.25).

Bainite shows a lamellar structure, which has from the morphology some similarities with martensite. Bainite commonly consists of ferrite, carbide, and retained austenite. In these cases it is similar in constitution to pearlite, but with the ferrite forming by a displacive mechanism similar to martensite formation, usually followed by precipitation of carbides from the supersaturated ferrite or austenite. The fact that the different microstructures possess different properties is technically very important. Steels can be optimized for different properties by chemical composition and heat treatment. The chemical compositions and designations of ferritic-martensitic steels for structural applications is shown in Table 2.3. In this table not only commercial grades were listed but also steels which are still in development or available as experimental batches only. It can be seen that different classes concerning chromium content exist:

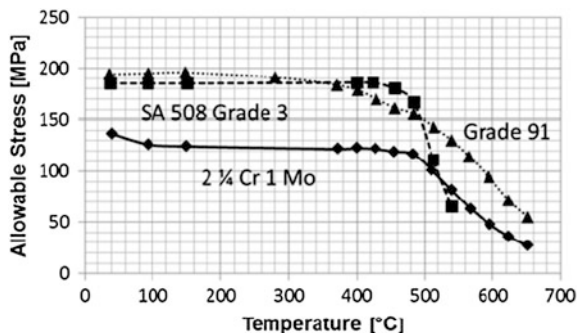
- Carbon steels
- Low chromium (2–3 %) chromium steels
- 9–12 % Cr steels

Chromium contents above 12 % also exist as being discussed for dispersion strengthened steels later.

High strength, high toughness and good weldability are requirements for reactor pressure vessels. As the pressure vessel material temperature in light water reactors remains limited to below 320 °C high temperature strength is not a requirement and low-alloy ferritic and bainitic steels such as A533B (nominally Fe-1.25Mn-0.5Ni-0.5Mo-0.2C, see Table 2.3) are used for the pressure boundary components.

For advanced reactors as proposed by GEN IV higher vessel or pressure vessel temperatures are envisaged requiring improved high temperature strength. The ferritic/bainitic 2 1/4 Cr 1Mo steel which has more alloying elements would be a candidate material which is in fact used as the RPV material for the Japanese gas cooled reactor HTTR. But also this steel could not be used without limitations for temperatures envisaged for a hot vessel of a very high temperature reactor. This is only possible with advanced martensitic steels like Grade 91 (see Fig. 2.26 [29]).

Fig. 2.26 Design stresses for different pressure vessel steels: carbon steel, low alloy steel, martensitic 9 % Cr steel. Allowable stress means that for these stresses the materials can be used at the respective temperatures for a design life of 3×10^5 h [29]. Details about establishing such curves are given in Chap. 8



2.3.1.1 9–12 % Chromium Steels

Best high temperature strength in the class of 2–12 % chromium steels possess the martensitic 9–12 % chromium steels. This class of steels belong due to its superior strength, creep rupture strength and radiation properties (discussed later) to the most important type of materials for future nuclear plants. The fact that it is iron based and therefore not too expensive (compared with nickel based alloys) makes it also very attractive for non-nuclear components acting at elevated temperatures (e.g. coal gasification, supercritical steam turbines). As a result of extended research and development the stress rupture properties of the class of martensitic 9–12 % chromium steels could be significantly improved. This class of materials has been extensively reviewed in the literature particularly with respect to nuclear applications in [30, 31]. High-chromium (9–12 % Cr) ferritic/martensitic steels were first considered for elevated-temperature in-core applications (cladding, wrappers, and ducts) for fast reactors in the 1970s, because of their excellent thermal properties and irradiation resistance (low swelling) relative to austenitic stainless steels. Sandvik HT9, nominally Fe-12Cr-1Mo0.5 W-0.5Ni-0.25 V-0.2C which was developed in Europe in the 1960s for the power-generation industry, was chosen as the material for fast reactor programs in several countries. A large amount of information was generated in the respective nuclear programs on the properties of these steels before and after irradiation. When ferritic/martensitic steels were considered as structural materials for fusion reactors in the late 1970s, Sandvik HT9 was the first one considered in the U.S., in Europe and Japan. In the mid-1980s, the idea of low-activation materials was introduced into the international fusion programs. The objective was to build plants from materials that would either not become active when irradiated by neutrons or, if activated, develop low-level radiation or the radioactivity would decay quickly, allowing for improved safety of operation as well as hands-on maintenance. Truly “low-activation” steels defined in this way are not possible, because they are limited by the decay of the products from transmutation of iron atoms. “Reduced-activation” steels, where the activity decays in a relatively short

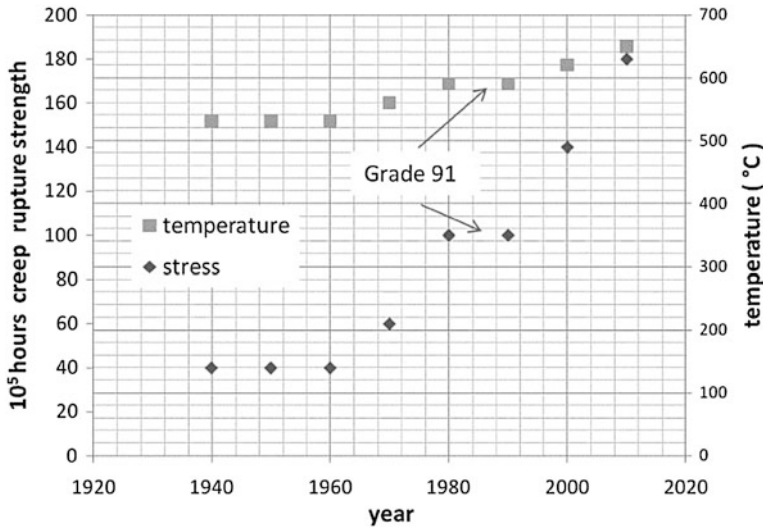


Fig. 2.27 Development of maximum service temperature and 10^5 h creep rupture strength of 9–12 % Cr steels over the years. Grade 91 steel is currently considered as a candidate for nuclear applications including reactor pressure vessel of a very high temperature reactor (VHTR) or gas cooled fast reactor (GFR) (after[31])

time, thus allowing for shallow land burial, as opposed to deep geological storage, were considered possible, and their development was pursued.

Due to its importance for technical applications we would like to mention the most important development steps of this class of steels following a very substantial overview over the class of ferritic-martensitic steels [31]. Generally, the microstructures of the 9 and 12 % Cr steels are designed by balancing austenite and ferrite stabilizers to produce 100 % austenite during austenitization and 100 % martensite during a normalizing (air cooling) or quenching treatment following austenitization. In some 12 % Cr-steels a small amount of δ -ferrite may be present. Some duplex steels containing martensite and δ -ferrite have been developed and used. The steel T91 has been used most extensively in power-generation industry throughout the world [32–34]. This grade is also considered as a candidate for generation IV fission plants in different applications. There exist also newer grades like Grade 92 or E911. They were developed and introduced in the 1990s for 620 °C operation with 10^5 h creep rupture strengths at 600 °C of 140 MPa. Further developments like the SAVE 12 or NF 12 were intended to raise the operating temperature up to 650 °C which can be considered as the maximum temperature which can be reached with this class of materials due to the thermal stability of the martensite. These developments were mainly triggered by the fossil

industry (e.g. coal gasification). Figure 2.27 shows the improvements of the creep rupture strength at the related maximum temperatures. The left scale refers to the stress corresponding with 10^5 h rupture life. The right scale refers to the related temperature. The martensitic steel qualities available until 1960 allowed only stresses of 40 MPa at a maximum temperature of 530 °C. Currently, at about 650 °C the 10^5 h can be reached with a stress of 180 MPa which is a significant improvement. These improvements could be achieved by a careful balance of alloying elements which have an influence on microstructure and microstructural stability.

Effect of Carbon and Nitrogen

Carbon and nitrogen are strong austenite stabilizers with a relatively large solubility in austenite. They have a very small solubility in ferrite, which gives rise to the formation of carbides, nitrides, and carbonitrides.

Effect of Chromium

Chromium is a ferrite-stabilizing element that is generally added to steels for oxidation and corrosion resistance. Chromium reacts with carbon to form carbides (M_7C_3 and $M_{23}C_6$). In steels containing nitrogen, chromium-rich M_2X (Cr_2N) can also form.

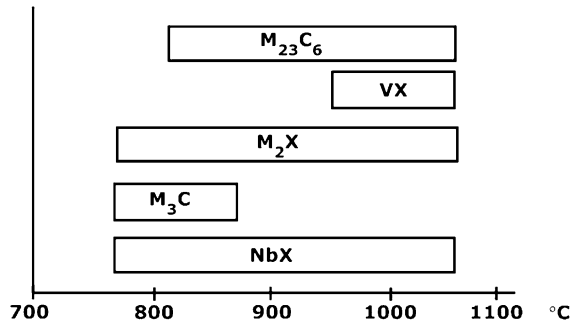
Effect of Tungsten and Molybdenum

Molybdenum and tungsten are ferrite stabilizers. They played an important role in the development of modern martensitic steels and for the development of reduced-activation steels for fusion applications. For further information we would like to refer to the literature [30, 31]

Effect of Vanadium and Niobium

Vanadium and niobium are strong carbide, nitride, and carbonitride formers, and in the 9–12 Cr steels, they are expected to form MX (M stands for metal), where V and Nb are enriched in the M, and X is either carbon, nitrogen, or a combination of the two, resulting in carbides (MC), nitrides (MN), or carbonitrides [M(C,N)].

Fig. 2.28 Evolution of precipitates in martensitic steels with tempering temperature, M stands for metal (after[35])



Effect of Boron and Phosphorus

Boron is a surface-active element with a low solubility in ferrite, and it is often used to increase hardenability. In many of the 9–12 % Cr steels, about 0.005–0.01 % B is added. It has been found to segregate to the surface of the $M_{23}C_6$ and decrease the rate at which the carbide can coarsen, thus stabilizing the microstructure, since the $M_{23}C_6$ helps pin the subgrain boundaries.

Effect of Nickel, Manganese, and Cobalt

Nickel, manganese, and cobalt are austenite stabilizers. The main reason for adding them to 12 Cr steels is to ensure 100 % austenite formation (no δ -ferrite) during the austenitization treatment, thus ensuring 100 % martensite when cooled. Nickel and manganese have been shown to have a strong solid-solution strengthening effect in iron.

Effect of Copper

Copper is an austenite-stabilizing element, but it is different from Ni, Mn, and Co in that it has a low solubility in ferrite. It can remain in solution during a normalization or quenching treatment, but it will precipitate during tempering and aging. Copper precipitation can strengthen the steel and can play a role in the nucleation of other phases during thermal aging or creep.

For nuclear fission applications (hot vessel for VHTR/GFR, core support structures, claddings etc.) grade 91 is considered as the most important martensitic steel. However, more advanced creep resistant steels are certainly candidates for supercritical steam turbines which can be used together with advanced nuclear reactors. These steels are commonly used in a “normalized and tempered” condition. This heat treatment involves a solutionizing treatment (austenitizing) that produces austenite and dissolves the carbides, followed by an air cool that transforms the austenite to martensite. The austenitization plus air cool is referred to as

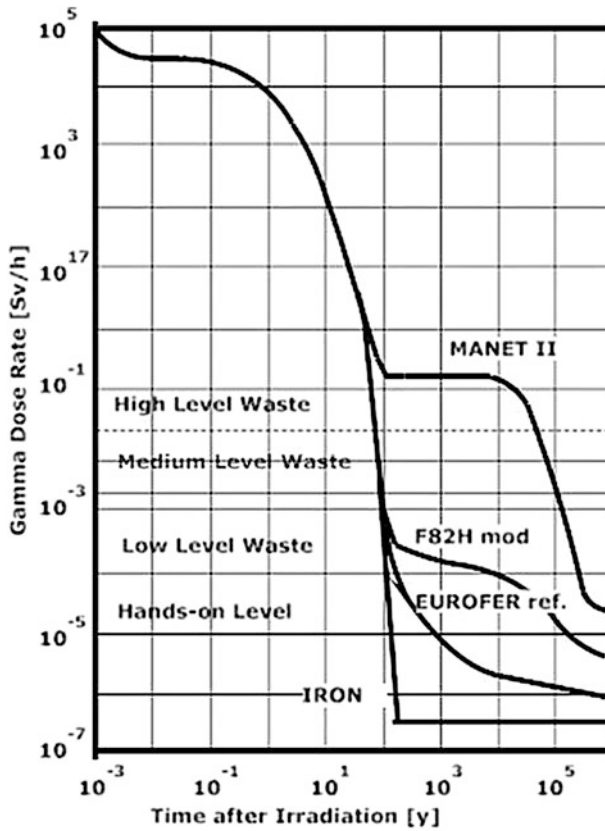


Fig. 2.29 Calculated development of dose rate at the surface of irradiated samples. Manet II, F82H mod and EUROFER are low activation martensitic steels, EUROFER shows the lowest activation after irradiation. (replotted after [36, 37])

the normalization treatment. Typical normalized microstructures consist of a martensite lath network. In commercial practice, the normalized steels are tempered by heating between 650 and 780 °C. Although the microstructures after tempering appear similar to the normalized microstructure transmission electron microscopy shows a variation in structure, depending on the tempering conditions. For the high-temperature tempering treatment generally used (650–780 °C) the “tempered martensite” consists of a ferrite matrix with carbide precipitates. These precipitates have a strong influence on the elevated temperature properties of such steels. Figure 2.28 shows the precipitate evolution with tempering temperature [35]. The X indicates that carbides, nitrides or carbo-nitrides are formed. Under certain circumstances nano-sized carbo-nitrides can be formed in martensitic steels which can significantly improve the high temperature strength of these materials which will be further discussed later in this chapter.

Martensitic steels are of interest also for the blanket in a fusion reactor. Materials in a fusion reactor are exposed to very high radiation levels which cause activation of the materials when certain elements are present as is already discussed briefly above, which is a problem with respect to radioactive waste. A major activity of the fusion research is therefore reduction of the alloying elements and impurities which can be activated and to improve strength and helium distribution by dispersoids (discussed later in this chapter). One strategy in this respect is replacing niobium by tantalum and molybdenum by tungsten.

This led to the development of EUROFER [38] with contents of Nb, Mo, Ni, Cu, Al and Co restricted to ppm-values. Figure 2.29 [36] shows the development of γ -radiation dose rates of different steels after neutron radiation with a spectrum typical for a fusion reactor first wall compared with iron. It can be seen that current qualities (EUROFER) match the disposal requirements. Introduction of dispersoids increases also the strength of the material to acceptable levels as summarized in [36, 37].

2.3.1.2 Bainitic Steels

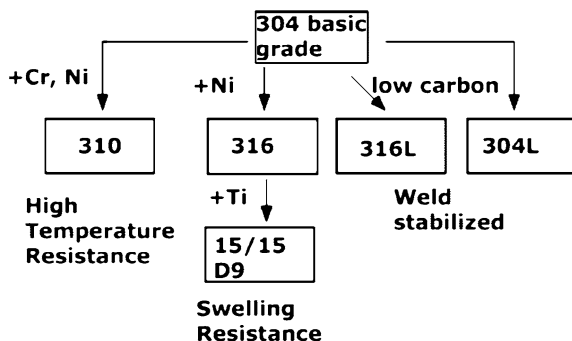
The search for low activation materials had also an influence on research for improvement of lower chromium (2–3 %) steels. This work was primarily done at Oak Ridge [39] in connection with research on fusion materials. When the chromium concentration is reduced from 9 % to 2–3 %, the tendency to form martensite (hardenability) is reduced. For a given section size, this means that for such a steel to form martensite, it must be cooled significantly faster from the austenitization temperature than a 9 % Cr steel. As a result, martensite is not expected to form in section thickness over a few millimeters. Instead, bainite forms. However, if the section thickness is large enough or the hardenability is small enough, the bainite will be accompanied by ferrite. Besides improvements of the 2 ¼ Cr 1Mo steels the 3 % chromium steels were studied. As a result of these studies, a steel was produced with base composition nominally Fe-3.0Cr-3.0 W-0.25 V-0.10C (3Cr-3WV). An addition of 0.07 % Ta (3Cr-3WVTa) to this base composition was found to further improve strength and toughness. However, they were only as experimental batches produced. (see Table 2.3 for nominal compositions). Preliminary tests on the steel indicate that this bainitic steel develops a combination of strength and toughness that would appear to make it a suitable candidate for pressure vessels, piping, and other pressure boundary components of Generation IV reactors. The steel is considered as a possible replacement for 2 1/4Cr-1Mo and modified 9Cr-1Mo steels in the petrochemical and power-generation industries. In the section sizes investigated to date, the 3Cr-3WV steel has very high strength. Additionally, the Charpy impact toughness of the steels is as good or better than that of A533 grade B class 1 plate (i.e. the well known PWR/BWR pressure vessel steel). In addition to these advantages, a 3Cr-3WV-type steel would also offer advantages for plant operation. Present A533 grade B Class 1 and A508 Grade 2/3 Class 1 LWR vessels are clad with stainless steel to prevent

corrosion products from contaminating the coolant. The higher chromium level of the 3Cr-3WV makes it more corrosion resistant, perhaps allowing it to be used without cladding. The higher chromium means the steel is also more resistant to hydrogen embrittlement. Based on observations on various higher-alloyed ferritic steels (e.g., 2 1/4Cr-1Mo, modified 9Cr-1Mo, Sandvik HT9) irradiated to high doses this 3Cr-3WV steel should be highly resistant to irradiation embrittlement compared to the current LWR steels. This might allow a reactor to be operated to a higher fluence with a smaller coolant gap, which means a smaller-diameter vessel, all other conditions being equal for the two steels. Because of its better elevated-temperature properties, components could be operated at higher temperatures than those for current LWRs, with a concomitant increase in efficiency. Furthermore, the composition of the 3Cr-3WV steel complies with the “reduced activation” criteria established in the fusion program. Current reactor pressure vessel steels contain significant amounts of radiation-sensitive elements, such as nickel and molybdenum, which result in significant activation of the steel, and stainless steel cladding, which results in even higher activities. Reduced-activation materials contain only elements that, when activated during service, rapidly decay (typical long-decay alloying elements Ni, Nb, Cu, and Mo are eliminated from the composition). In the fusion program, the objective for these steels is to allow shallow land burial of components after service. Although shallow land burial of LWR pressure vessels is already allowed (due to lower doses than a fusion plant), this material could provide additional safety margin in that regard. Of course, fabrication and irradiation effects are issues that would need to be resolved, in addition to inclusion within design codes [40].

2.3.1.3 Austenitic Steels

The austenitic matrix can be stabilized at room temperature by additions of specific alloying elements as shown in the Scheffler Diagram (Fig. 2.23). Austenitic steels have a face-centered cubic crystal structure and they are not magnetic. Because of its high chromium and nickel contents these steels have superior corrosion resistance and are therefore used in LWR environment as reactor internals. They show also creep properties exceeding the ones of the ferritic-martensitic steels at high temperatures. The problem is that they have a low yield strength compared with ferritic-martensitic steels. They are therefore often used in the cold worked condition. Cold working increases the dislocation density in these steels which leads to high distortion of the lattice and the existing dislocation structure impedes further dislocation movement thus increasing the yield stress. The austenitic stainless steels, because of their high chromium and nickel content, are most corrosion resistant steels. For nuclear applications the types 316, 304 and 15/15 are most important. The 304/316 group contains at least 16 % chromium and 6 % nickel (the basic grade 304 is referred to as 18/8) and range through to the high alloy or “super austenitics” such as 904L and 6 % molybdenum grades. Additional elements can be added such as molybdenum, titanium or copper,

Fig. 2.30 Development tree of different austenitic steels (see also [41])



to modify or improve their properties, making them suitable for many critical applications involving high temperature as well as corrosion resistance. This group of steels is also suitable for cryogenic applications because the effect of the nickel content in making the steel austenitic avoids the problems of brittleness at low temperatures, which is a characteristic of other types of steel.

The relationship between the various austenitic grades is shown in Fig. 2.30. Type 304 is the most common of austenitic grades, containing approximately 18 % chromium and 8 % nickel. It is used for LWR reactor internals, for chemical processing equipment, for food, dairy, and beverage industries, for heat exchangers, and for the milder chemicals. Type 316 contains 16–18 % chromium and 11 % to 14 % nickel. It also has molybdenum added to the nickel and chrome of the 304. The molybdenum is used to control pitting corrosion. It is used in similar applications like 304. Different grades are used to describe additional properties. The “L” grades are used to provide extra corrosion resistance after welding. The letter “L” after a stainless steel type indicates low carbon (as in 304L). The carbon is kept to 0.03 % or less to avoid chromium-carbide precipitation on the grain boundaries. This maintains the chromium in solution and promotes corrosion protection adjacent to the grain boundaries. Also for better weldability, the “L” grades are used. These grades are basically within the basic specifications but to meet the specific properties they are usually more expensive because a tighter chemical composition must be met. The “H” grades contain a minimum of 0.04 % carbon and a maximum of 0.10 % carbon and are designated by the letter “H” after the alloy. The “H” grades are used for high temperature application as the higher carbon helps the material retain strength at rather high temperatures.

Austenitic steels suffer from void swelling under irradiation as shown in Chap. 5. The austenitic material with best resistance against swelling is a titanium modified 316, also known as Alloy D9 (15 %Cr-15%Ni-0.2 %Ti), in the 20 % cold-worked condition [42] (see also Chap. 5). Austenitic stainless steels are still favoured (particularly in India) for fuel pin cladding and other core component applications since they possess the required strength characteristics up to 923 K. Early studies on creep properties [43] of alloys with titanium to carbon ratio between 4 and 6 showed that titanium content strongly influences the creep rupture life. However, the limiting factor at moderate reactor operating temperatures of up to ~600 °C is

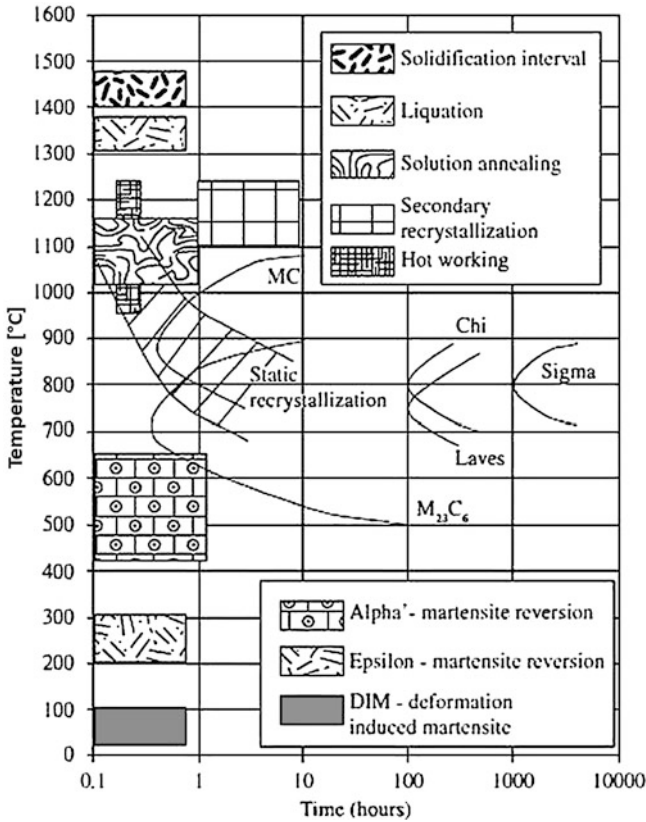


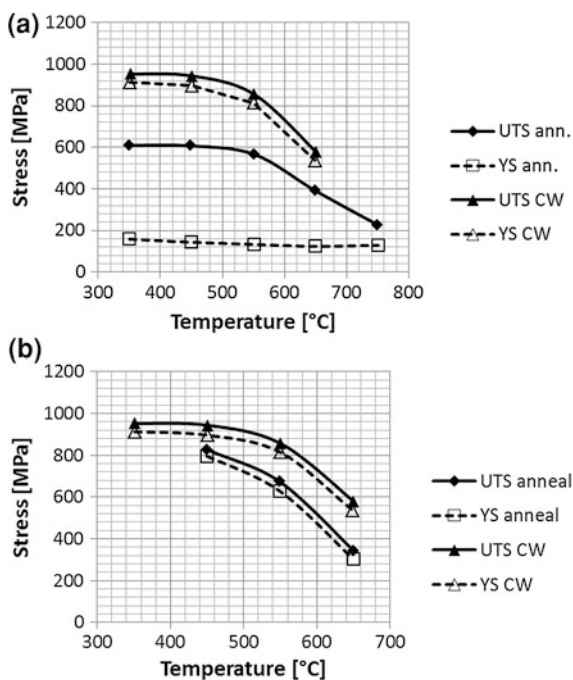
Fig. 2.31 Main transformations that occur in austenitic stainless steels between room temperature and the liquid state. (source [44]). With permission of “key to metals”

void swelling which ultimately limits life of the fuel pin leading to a reduced burn-up of about 100 GWd/tonne (Gigawatt-days per tonne is a measure of the energy extracted from a metric ton of nuclear fuel. 1 GWd corresponds to 86.4×10^{12} J or 24 million kWh of electricity [42]).

Similar to ferritic martensitic steels also the austenitic steels start to precipitate different phases when exposed to high temperatures for a certain time. Figure 2.31 gives an overview about the general behaviour of austenites [44].

Below about 1,300 °C the steel is out of the solid/liquid regime and it is in a solid state. In the temperature interval between about 950 and 1,250 °C hot working operations are performed. About the same temperature interval is used for solution annealing where several carbides and other precipitates are dissolved in the matrix. Solution annealing is an important step in the whole heat treatment sequence to obtain optimum materials properties. At lower temperatures reversion of alpha' and epsilon martensite (specific forms of martensite which are not further discussed here) takes place [45]. Between room temperature and 100 °C

Fig. 2.32 **a** Yield stress and ultimate tensile stress of SS316 in annealed (ann) and in 20 % cold worked (CW) condition at different test temperatures. **b** Yield stress and ultimate tensile stress of SS316 in 20 % cold worked condition (CW) and after 4,000 h annealing (anneal) at test temperature

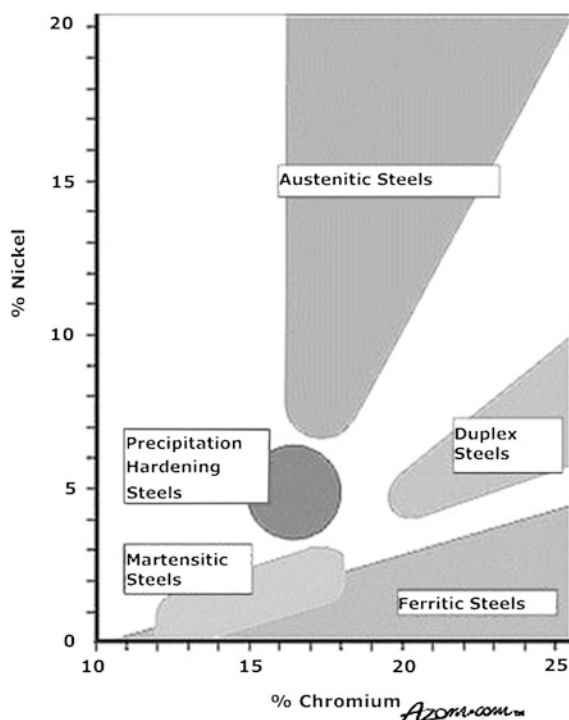


deformation induced martensite can form which is considered as a quantitative measure for deformation of the material (see e.g. [46]). Maintaining the material for longer times at high temperatures can lead to recrystallization (secondary or static) and to precipitation of different phases Carbides (MC , $M_{23}C_6$), Laves, Chi and Sigma. The appearance of these phases can deteriorate long-term properties (creep strength, ductility). Increasing yield strength and tensile strength by cold working remains only effective until certain temperature. Figure 2.32 a shows the influence of a 20 % cold deformation on the strength of a 316 steel [47]. A remarkable increase in yield strength and ultimate tensile strength was found when comparing annealed with the 20 % cold-worked conditions. This high strength is a result of high dislocation density and dislocation arrangement produced by the massive cold deformation. The problem is that this dislocation arrangement recovers with increasing temperature leading to a loss of hardening as shown in Fig. 2.32b. This implies that cold working can be used to improve the strength of austenitic material only for temperatures occurring in light water reactors.

2.3.1.4 Duplex Stainless Steels

Duplex stainless steels carry this name because their microstructures consist of both, austenitic and ferritic phases. They show therefore also characteristics of

Fig. 2.33 Classes of stainless steels (copyright Azom)



both types of these steels which make them very attractive for different applications. The main properties of duplex steels can be summarized as follows: Duplex steels have much better tensile properties than austenitic or ferritic steels. In most cases they also have better toughness and ductility than ferritic steels, however, they do not reach the excellent values of austenitic steels. Duplex stainless steels are extremely corrosion resistant, resistant to stress corrosion cracking and work hardenable alloys.

2.3.1.5 Precipitation Hardening Stainless Steels



These are chromium and nickel containing steels that can develop very high tensile strengths up to elevated temperatures. The most common grade in this group is “17-4 PH”, also known as Grade 630, with the composition of 17 % chromium, 4 % nickel, 4 % copper and 0.3 % niobium. The great advantage of these steels is that they can be machined in the (softer) solution treated condition. Following machining, forming etc. the steel can be hardened by a one-step ageing heat-treatment at fairly low temperature which causes no distortion of the component. Precipitation-hardened stainless steels possess good corrosion resistance and excellent mechanical properties and are also amenable to conventional fabrication

processes. Depending on the austenite stability at ambient temperatures, they can be classified into three classes: austenitic, semi-austenitic and martensitic steels. Precipitation hardening is generally achieved in these steels from homogeneously nucleated fine precipitates of intermetallic or elemental phases [48, 49]. Figure 2.33 shows as a summary chromium and nickel contents of the different classes of steels which are also known as stainless steels. Several of them play an important role in current and in advanced nuclear plants. Duplex and precipitation hardened stainless steels are mainly used to provide corrosion resistance at lower temperatures.

2.3.2 Superalloys

For higher temperatures other strengthening mechanisms must be activated. Changing the matrix from iron to nickel or cobalt leads to a new class of alloys which are called \ll superalloys \gg . Most important properties of superalloys are high temperature strength and creep resistance. Other crucial material properties are fatigue life, phase stability, as well as oxidation and corrosion resistance. High creep resistance is used for high temperature applications like intermediate heat exchangers (IHX) in advanced gas cooled reactors. As cobalt (easily to activate hard gamma radiator) is not welcome in nuclear applications in this book only with nickelbase superalloys shall be dealt with. Also nickel is not without problems in a radiation environment because it can be converted by nuclear reactions to an alpha emitter, which means that gaseous helium can become present in the material, a situation which will be described more in detail in the radiation damage section. Nickel-base superalloys are primarily nickel alloys containing substantial quantities of chromium, cobalt, refractory elements such as molybdenum and tungsten, and titanium together with Al. Besides solid solution strengthening the way for particle strengthening was opened by the discovery of precipitation of the gamma prime phase (γ'), Ni_3Al , in an austenitic iron-nickel alloy before World War II. Precipitation hardened superalloys are very difficult to machine and many of them are too brittle for forging, which means that they have to be cast (precision cast). Driving force for the development of this class of materials was the need for high strength, high creep resistant alloys for jet engines at temperatures of about 700 °C. The alloy A-286 which is still in use was one of the first commercial available austenites which could be strengthened by γ' . Essential solutes in γ' hardening nickel based superalloys are aluminium and/or titanium, with a total concentration which is typically less than 10 atomic percent. This generates a two-phase equilibrium microstructure, consisting of gamma (γ) and gamma-prime (γ'). The γ -phase is a solid solution with fcc lattice and a random distribution of the different species of atoms. By contrast, γ' is an ordered intermetallic phase with an fcc lattice in which the nickel atoms are at the face-centres and the aluminium or titanium atoms at the cube corners. The partitioning of different other elements within the microstructure is shown schematically in Fig. 2.34. Table 2.4 lists the

IIA	IIIA	IVA						
	B	C						
	Al		IVB	VB	VIB	VIIB	← VIIIIB →	
		Ti	V	Cr		Fe	Co	Ni
	Y	Zr	Nb	Mo		Ru		
		Hf	Ta	W	Re			

 partitions to γ'
 partitions to GB


 partitions to γ

Fig. 2.34 Partitioning of the most important elements in superalloys (after [53])

chemical compositions of superalloys important for nuclear applications. The γ' phase is mainly responsible for the elevated-temperature strength of the material and its very high resistance to creep deformation. Although γ' is a nickel aluminide the presence of titanium has an important influence on the development of this phase as shown in Fig. 2.35. For a given chemical composition, the fraction of γ' decreases as the temperature is increased. This phenomenon is used to dissolve γ' at a sufficiently high temperature (a solution treatment) followed by ageing at a lower temperature to generate a uniform and fine dispersion of strengthening precipitates. This atomic arrangement has the chemical formula Ni_3Al , Ni_3Ti or $\text{Ni}_3(\text{Al,Ti})$. In addition to aluminium and titanium, niobium, hafnium and tantalum partition preferentially into γ' . The high amount of alloying elements make superalloys prone to formation of many different phases with exposure time of which some can embrittle the material which will be discussed in context with the alloy IN-617.

In summary the following phases are present in most nickelbase superalloys (after [50]):

- Gamma (γ): The continuous matrix which is a face-centered nickel-based austenitic phase that contains a high percentage of solid solution elements as previously mentioned.
- Gamma Prime (γ'): Is the primary strengthening phase. It is an intermetallic (ordered) phase with typical composition $\text{Ni}_3(\text{Al,Ti})$. It is a coherently precipitating phase. This means that the crystal planes of the precipitates are in registry with the matrix. The lattice parameters of matrix and precipitates differ only slightly which, together with the chemical compatibility, allows a homogeneous precipitation throughout the matrix. The yield stress of the gamma prime phase increases with temperature up to about 700 °C. This is a result of dislocation movement through the ordered crystal which shall not be further discussed here.

Table 2.4 Chemical compositions of nickel–iron based superalloys for nuclear applications

	C	Ni	Fe	Si	Mn	Co	Cr	Ti	Mo	Al	B	Others
IN-617	0.05–0.15	Bal.	Max. 3.0	Max. 0.5	Max. 0.5	10.0–15.0	20.0–24.0	Max. 0.6	8.0–10.0	0.8–1.5	Max. 0.006	Ou max. 0.5
HA-230	0.1	57	Max. 3.0	0.4	0.5	5	22		2	0.3	Max. 0.015	W 14 La 0.02 V 0.1–0.5
A-286	Max. 0.08	24.0–27.0	Bal.	Max. 1.0	Max. 2.0	–	13.5–16.0	1.9–2.35	1.0–1.5	Max. 0.35	0.003–0.010	
Hastelloy X	0.1	47	18	Max. 1	Max. 1	1.5	22		9		Max. 0.008	W 0.6
Hastelloy XR	0.07	Bal.	18.3	0.31	0.9	Max. 0.05	21.7	Max. 0.05	8.97	Max. 0.05	Max. 0.001	N 0.006
Hastelloy N	Max. 0.08	71.0	Max. 5.0	Max. 1.0	Max. 0.80	Max. 0.20	7.0	Al + Ti max. 0.35	16.0	Ai + Ti max. 0.35	–	Ou max. 0.35 W Max. 0.5
X-750	Max. 0.08	min. 70	5.0–9.0	Max. 0.5	Max. 1	Max. 1.0	14.0–17.0	2.25–2.75	Max. 1.0	0.4 1.0	Max. 0.001	Nb + Ta 0.7–1.2
IN-600	0.15	72.0	8.0	0.5	1.0							Ou 0.5 S 0.015
IN-718	0.045	53.4	18.5	0.35	0.35	1.0	18.5	1.0	3.0	0.5		Nb 5.0
IN-800	Max. 0.1	30.0–35.0	min 39.5				19.0–23.0	0.15–0.6		0.15–0.6		Al + Ti 0.3–1.2
IN-800H	0.05–0.1	30.0–35.0	min 39.5				19.0–23.0	0.15–0.6		0.15–0.6		Al + Ti 0.3–1.2

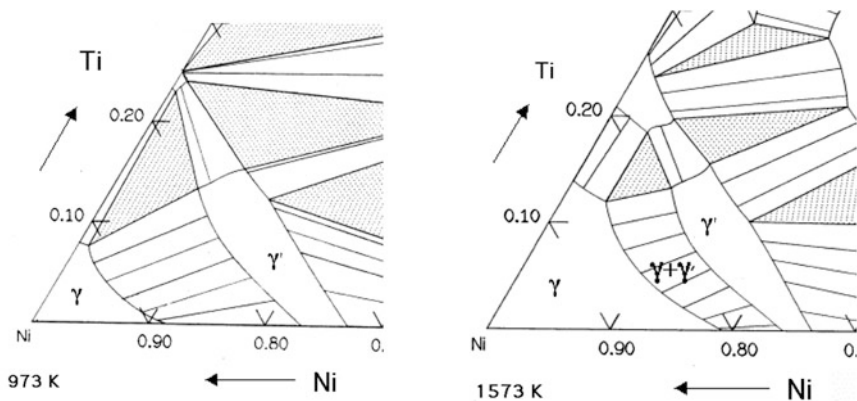


Fig. 2.35 Influence of titanium content and temperature on the γ' formation (with permission of « key-to metals » [51])

Nickelbase superalloys are available with a wide range of γ' volume fractions. Modern high strength nickelbase superalloys for gas turbine blades and vanes contain γ' volume fractions of 70 % and more. The particles provide obstacles for the movement of dislocations which leads to the increase in strength, particularly at higher temperatures. Depending on particle size and temperature dislocations can surround, cut or overclimb them.

- **Carbides:** Carbon, added at levels of 0.05–0.2 wt. % combines with reactive and refractory elements such as titanium, tantalum, and hafnium to form primary MC carbides (e.g. TiC, TaC, or HfC). They are called « primary » because they precipitate already from the melt. They are not dissolved during solution heat treatments. Other carbides such as $M_{23}C_6$ and M_6C can be formed predominantly along grain boundaries during heat treatment. All these carbides have a fcc crystal structure. These carbides can be advantageous as well as detrimental for the superalloy properties. As massive grain boundary precipitates they can reduce the cohesion of the grain boundaries thereby reducing toughness and ductility of the alloy on the one hand. On the other hand they can reduce grain boundary sliding during creep thereby increasing the creep strength of the alloy.
- **Topologically Close-Packed (TCP) Phases:** TCP-phases usually form platelets. The plate-like structure reduces ductility and creep properties. The cell structure of these phases has close-packed atoms in layers separated by relatively large interatomic distances. The layers of close-packed atoms are displaced from each other by sandwiched larger atoms, developing a characteristic « topology ». Therefore these compounds are called topologically closed packed (TCP) phases. Main representatives of these phases are σ , μ , and Laves Phase. They are generally undesirable brittle phases that can form during service. The sigma phase appears to be the most deleterious.

The high metallurgical flexibility of nickelbase alloys makes them useful for many technical applications. The high nickel and chromium contents make them corrosion resistant. Addition of aluminum promotes the formation of an aluminium oxide layer at high temperatures which makes such alloys resistant against further oxidation at very high temperatures (e.g. first stage blades and vanes in aeroengines and land-based gas turbines). Depending on the application composition and heat treatment can be chosen that no, or almost no gamma prime particles are precipitated. This class is called solid solution strengthened. They are normally used in applications where high corrosion resistance is required. High gamma-prime forming alloys are employed when high high-temperature strength is required. Further and more detailed information can be found in one of the numerous books on superalloys e.g. [52, 53].

According to this flexibility nickelbase alloys play also a very important role for current and advanced nuclear plants. Unfortunately, they suffer from a transmutation reaction of nickel producing helium when irradiated with fast neutrons. The presence of helium gas in the material deteriorates the mechanical properties which limits the application of these alloys to locations where no exposure to fast neutrons can happen. We will discuss these effects in more detail in the chapter on irradiation damage. In the following a few important nickel-base alloys for nuclear plants will be introduced.

Incoloy 800 is an iron-nickel based alloy. Increasing the nickel and chromium content in austenitic steels improved its high temperature strength and also corrosion resistance. The alloys *Incoloy 800*, *800H*, and *800HT* are iron-nickel-chromium alloys with good strength and excellent resistance to oxidation and carburization in high-temperature exposure. The nickel-iron-chromium alloy 800 was introduced to the market in the 1950s to fill the need for a heat- and corrosion-resistant alloy with a relatively low nickel content since nickel was, at the time, designated a “strategic” metal. The alloy *800H* was further developed to the higher creep and stress rupture resistant alloy *800HT*. *Incoloy alloy 800HT* has a restricted chemistry, within the limits of alloy *800H*, and requires a heat treatment of 1,149 °C minimum. The carbon is 0.06–0.10 % (alloy *800H* is 0.05–0.10 %), the Al + Ti is 0.85–1.20 % (alloy *800H* is 0.30–1.20 % Al + Ti). The 1.2 wt. % aluminum and titanium leads to the formation of gamma prime phase which improves the high temperature strength and the creep resistance. The nickel content makes the alloys highly resistant to both chloride stress-corrosion cracking and to embrittlement from precipitation of sigma phase. *Incoloy 800* is primarily used in applications with temperatures up to 600 °C, where alloys *800H* and *800HT* are normally used in temperatures above 600 °C where resistance to creep and stress rupture is required. The chemical balance allows the nickel alloy to exhibit excellent resistance to carburization, oxidizing and nitriding atmospheres. *Incoloy 800HT* is microstructurally very stable and it is not expected to become brittle even after long periods of usage in the 650–870 °C like other stainless steel qualities do. Excellent cold forming characteristics typically associated with the nickel-chromium alloys are exhibited with *800HT*. For nuclear applications alloys

of type 800 are important materials for heat exchangers, steam generators and they are also considered for control rods in high temperature gas cooled reactors [54].

Inconel X-750 is a Nickel-Chromium alloy made γ' -precipitation hardenable by additions of Aluminium and Titanium. It has good creep-rupture strength at high temperatures to about 700 °C. The alloy Inconel X-750 is used worldwide as material for fasteners and centering pins in core internals and core components of water-cooled reactors-pressurized-water reactors (PWRs) as well as boiling-water reactors (BWRs).

Inconel alloy 600 is a standard engineering material for applications which require resistance to corrosion and heat. The alloy also has excellent mechanical properties and presents the desirable combination of high strength and good workability. The chemical composition of Inconel alloy 600 is shown in Table 2.5. The high nickel content gives the alloy resistance to corrosion by many organic and inorganic compounds and also makes it virtually immune to chloride-ion stress-corrosion cracking. Chromium confers resistance to sulfur compounds and also provides resistance to oxidizing conditions at high temperatures or in corrosive solutions. The alloy is not precipitation hardenable; it is hardened and strengthened only by cold work. The versatility of Inconel alloy 600 has led to its use in a variety of applications involving temperatures from cryogenic to above 1,100 °C. The alloy is used extensively in the chemical industry for its strength and corrosion resistance. Applications include heaters, stills, bubble towers and condensers for processing of fatty acids; evaporator tubes, tube sheets and flaking trays for the manufacture of sodium sulfide; and equipment for handling abietic acid in the manufacture of paper pulp. The alloy's strength and oxidation resistance at high temperatures make it useful for many applications in the heat-treating industry. It is used for retorts, muffles, roller hearths and other furnace components and for heat-treating baskets and trays. In the aeronautical field, Inconel alloy 600 is used for a variety of engine and airframe components which must withstand high temperatures. Examples are lockwire, exhaust liners and turbine seals. Inconel alloy 600 is used in the electronic field for such parts as cathode-ray tube spiders, thyatron grids, tube support members and springs. The alloy is a standard material of construction for nuclear reactors. It has excellent resistance to corrosion by high-purity water, and no indication of chloride-ion stress-corrosion cracking in reactor water systems has been detected. For nuclear applications, the alloy is produced to exacting specifications and is designated Inconel alloy 600T [55].

The IN 617 alloy (composition see Table 2.6) is largely a solid-solution strengthened nickel-base superalloy introduced in the early 1970s [56] that is well known for its good oxidation and corrosion resistance at temperatures up to 1,100 °C and high creep-rupture strength at temperatures from 650 to 1,100 °C. The Al in conjunction with Cr provides oxidation resistance at high temperatures. Furthermore, the presence of Al leads to additional strengthening through the precipitation of the γ' intermetallic upon extended aging at intermediate temperatures, [57–59] over and above the solid solution strengthening imparted by Co and Mo. For example, aging of this alloy at 700–750 °C was found to cause precipitation of γ' , with a fine size of 20–90 nm and a volume fraction up to 4 pct.

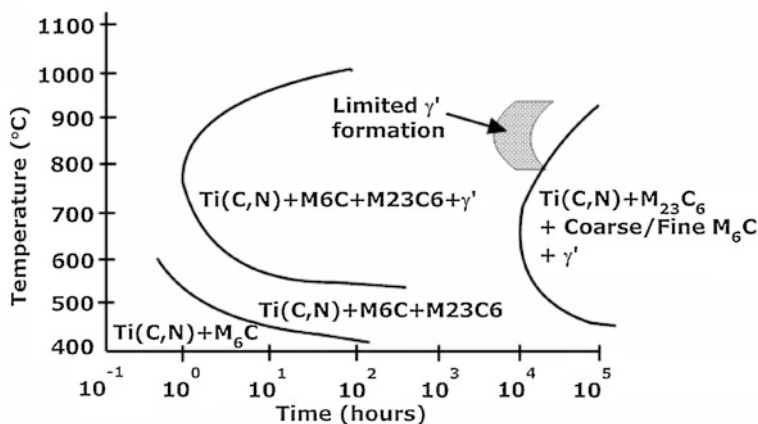


Fig. 2.36 Phases developing in IN-617 as a function temperature and time [58]

Apart from these features, some strengthening of the alloy is also derived from the formation of carbides of the types $M_{23}C_6$, eta- M_6C , and $Ti(C,N)$ as shown in Fig. 2.36. No topological close-packed phases, such as sigma (σ), mu (μ), or chi (χ), were found after aging at temperatures from 649 to 1,093 °C.

Haynes 230 is a solid solution strengthening superalloy comparable with IN-617 [60] and both alloys are under consideration as intermediate heat exchanger materials for a compact intermediate heat exchanger of a very high temperature gas cooled reactor [57].

The alloy *Hastelloy XR* is one example for materials development which was performed mainly with respect to improve the behaviour in a nuclear environment. The metal research at JAERI (today JAEA) for VHTR application initiated its essential activity in 1971 with basic explanatory investigations of critical problems to adopt existing alloys to very high temperature helium-cooled reactor systems. To improve the corrosion resistance in high temperature reactor helium the conventional solid solution strengthened superalloy *Hastelloy X* was manufactured as an aluminum free alloy with reduced cobalt and optimized manganese and silicon contents. The designation of this material was *Hastelloy XR*. The improvement was primarily achieved by the formation of stable and adherent surface layers consisting of $MnCr_2O_4$ and Cr_2O_3 [61].

Hastelloy N was an alloy tuned to requirements of molten salt reactors. *Hastelloy N* is a nickel-base alloy that was invented at Oak Ridge National Laboratories as a container material for molten fluoride salts. It has good oxidation resistance to hot fluoride salts in the temperature range of 700–870 °C. *Hastelloy N* is a solution-strengthened nickel-base alloy that was developed for good strength and corrosion resistance at about 650 °C. No intermetallic compounds have been identified in this alloy, but carbides precipitate and cause modest changes in the properties. The alloy has good weldability and can be readily

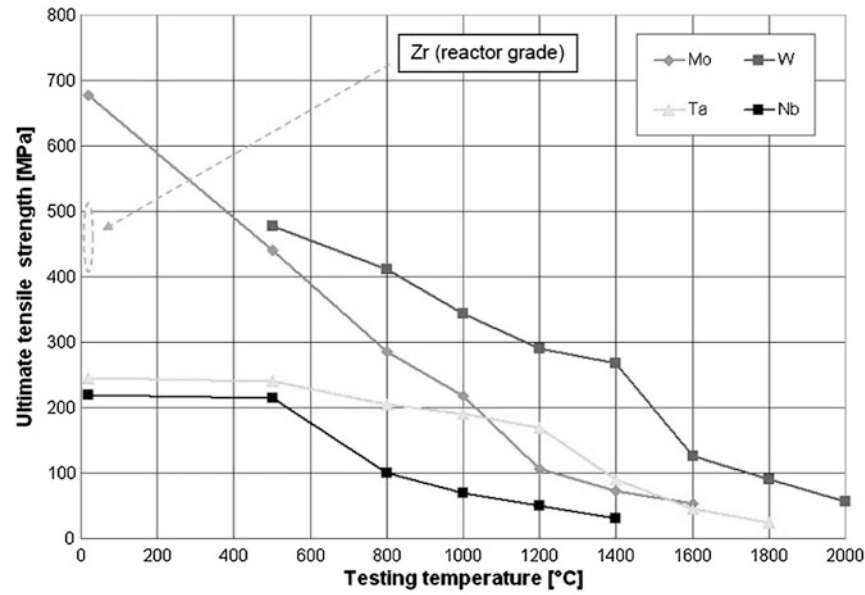
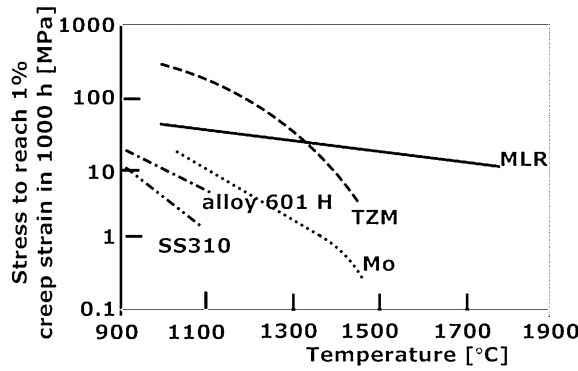


Fig. 2.37 Ultimate tensile strength of refractory metals [64] (Source Plansee)

Fig. 2.38 Creep properties of refractory metals and alloys compared with an austenitic steel and a superalloy. MLR represents a lanthana reinforced molybdenum alloy (replotted from [64])



forged. It has been successfully extruded and further processed into high-quality seamless or manufactured as welded and drawn tubing [62].

Highly creep resistant, gamma prime hardening nickelbase alloys are considered as candidates for a direct cycle gas turbine gas cooled reactors. Directionally solidified or single-crystalline cast materials (see Chap. 3) were proposed as blades and the forged alloys IN-718 or Udimet 720 were proposed as materials for the rotor disks in the turbine. Although no such turbine has been realized until now from experience with fossil fired gas turbines it can be expected that the proposed blades/vanes are a feasible choice. Forging of a large piece like a rotor disk might run into problems during the forging process. Nickelbase-alloys designed for very

good high temperature strength are difficult to deform by a high temperature process. This means that the through-forgability will make some troubles together with the low toughness of these alloys.

2.3.3 Refractory Alloys

The refractory metals include niobium (also known as columbium), tantalum, molybdenum, tungsten, and rhenium. Refractory metals have melting temperatures in excess of 2,000 °C. High temperature ultimate tensile strengths of different refractory metals are shown in Fig. 2.37. Hence, they should have potential applications at high temperatures. Figure 2.38 show the creep properties which indicate that although the application temperature can be high, the creep strength would not allow design of heavy loaded structural components. But the main obstacle for possible structural applications is the fact that refractory metals are readily degraded by oxidizing environments already at moderately low temperatures. This property has restricted the applicability of the metals to low-temperature or nonoxidizing high-temperature environments. Protective coating systems have been developed, mostly for niobium alloys, to permit their use in high-temperature oxidizing aerospace applications which last relatively short compared with nuclear power applications. Table 2.5 shows various aspects of refractory metals on a 10-point scale (1 being the worst and 10 being the best) [63]. This means that refractory metals are not really considered for advanced fission plants although they possess acceptable creep resistance and swelling resistance up to high burnups [63]. However, they are candidates for plasma facing components in fusion plants. Requirements for 1st wall materials are : high melting point, low interaction of the material with the plasma, resistance against cyclic loads. Refractory alloys are suitable in these respects and therefore molybdenum alloys (TZM), tungsten and tungsten-alloys are considered as divertor, tiles and other structural and functional parts in fusion plants like ITER [64]. The metals Ti, V, Cr, Zr, Hf, Ru, Rh, Os and Ir are counted to the enlarged group of refractory metals. In this group Zr, Ti and V are important for nuclear applications. Zirconium alloys will be introduced in the next section as important materials for LWRs and as a representative of titanium alloys the titanium aluminides will be discussed later. Vanadium alloys based upon the V-Cr-Ti system are studied as candidates for structural applications in fusion systems at intermediate temperatures because of their low activation properties, high thermal stress factor, good strength at elevated temperatures, and good compatibility with liquid lithium.

2.3.4 Zirconium Alloys

In the first test reactors (pool-type, water <100 °C) aluminium and beryllium alloys were used as cladding materials due to its low thermal neutron capture cross

Table 2.5 Some engineering properties of refractory alloys

Technology category	Nb-1Zr	Ta-10 W	TZM	W-Re	Re
Fabricability	8	7	4	3	4
Weldability	7	7	4	3	7
Creep strength	6	8	8	8	9
Oxidation resistance	1	1	3	3	7
Alkali metal compatibility	8	9	9	9	8
Radiation effects	6	6 ?	5	4	4 ?
Cost (2 mm sheet)	4	3	4	3	2

10 means highest potential, 1 means lowest potential. Alkali metal: Na, Li (*source* [63])

section. First nuclear power reactors (submarine propulsion) had higher thermal efficiency and because of its very low thermal neutron capture cross section zirconium was considered as a possible candidate. Zirconium has a high melting point (1,855 °C) and it is rather resistant against chemical attack. In contrast to the materials considered until now which had cubic structure (bcc or fcc) zirconium has a hexagonal close packed (hcp) structure. However, zirconium has poor ductility and resistance against reactor type corrosion as discussed in [Chap. 6](#) (hydrogen uptake). Additionally, zirconium occurs together with hafnium which had to be separated. Therefore stainless steel was introduced as cladding material in nuclear reactors. After world war II improvements in hafnium separation on a production scale were made. Additionally, it was found that Sn additions can significantly improve the corrosion behavior of zirconium. This material was called Zircaloy-1. Accidental contamination of a Zircaloy-1 batch with stainless steel residuals led to the discovery that additions of Fe, Cr and Ni could further improve the corrosion resistance (see [Chap. 6](#)). Main reason was the precipitation of (intermetallic) phases which were at least partly dissolved under irradiation thereby improving the oxidation resistance of the alloy. Beneficial in this respect are also additions of niobium. Currently, zirconium alloys are used for claddings in several water cooled reactors as shown in [Table 2.6](#). Main research concerning composition and microstructure of Zircalloys was with respect to oxidation, hydrogen up-take and radiation induced changes in geometry. These aspects will be discussed in [Chaps. 5](#) and [6](#). An important microstructure for nuclear applications is the so called “beta quenched” structure. The development of this structure during a heating-up and cool down cycle has been in situ monitored in a recent investigation [65]. This investigation is remarkable because it demonstrates how the advanced analytical tools available with high intensity synchrotron beamlines can be used to gain insight into metallurgical phenomena. A typical result of this investigation is shown in [Fig. 2.39](#). Heating up the cold rolled material led to the formation of recrystallized alpha grains. Further increasing the temperature promotes an alpha to beta transformation. Quenching finally leads to the typical beta quenched lamellar microstructure. More about manufacturing of claddings can be found in [Chap. 3](#).

Table 2.6 Typical chemical compositions and applications of Zircaloy

Alloy	Sn, %	Nb, %	Component	Reactor type
Zircaloy 2	1.2–1.71	–	Cladding, structural components	BWR
Zircaloy 4	1.2–1.7	–	Cladding, structural components	BWR, PWR, CANDU
ZIRLO	0.7–1	1	Cladding	PWR
Zr Sponge	–	–	Cladding	BWR
ZrSn	0.25	–	Cladding	BWR
Zr2.5Nb	–	2.4–2.8	Pressure tube	CANDU
E100	–	0.9–1.1	Cladding	RBMK
E125	–	2.5	Pressure tube	RBMK
E635	0.8–1.3	0.8–1	Structural components	RBMK
M5	–	0.8–1.2	Cladding, structural components	PWR

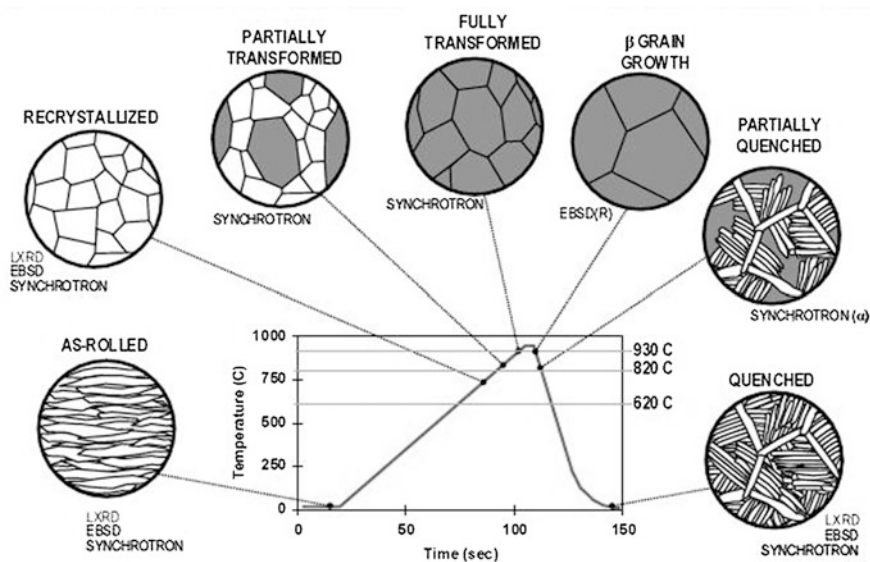
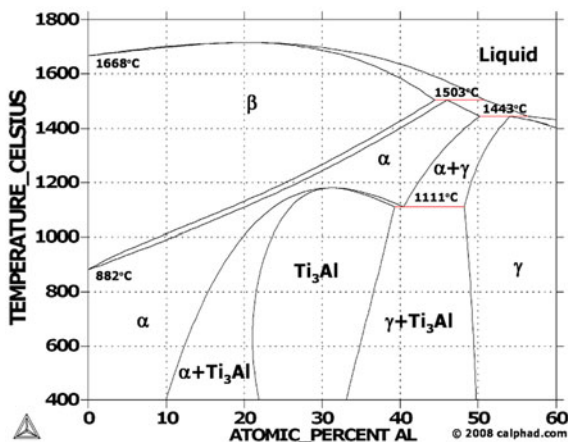


Fig. 2.39 Development of a beta quenched microstructure in Zircaloy. The different advanced investigation methods allowing in situ analyses: synchrotron, EBSD, electron backscatter diffraction; XRD and LXRD X-ray diffraction are described in [Chap. 7](#). Source [65], used with permission of Lars Hallstadius, Westinghouse

2.3.5 Intermetallics

Intermetallic phases are homogeneous chemical compounds between two or more metals. Although the main bonding type is metallic there are also elements of covalent and ionic bonding. The lattice shows an ordered structure which is in contrast to solid solution. Intermetallic compounds can have stoichiometric composition or the phase diagram may show areas where a homogeneous microstructure exists. Many intermetallic phases can occur in alloys as precipitates.

Fig. 2.40 Binary phase diagram of titanium and aluminum (with permission of: Calphad <http://www.calphad.com/titanium-aluminum.html>)



Some of them received quite some attention as structural materials. Most important in this respect are primarily the aluminides and to some extent also silicides.

- Nickel aluminides, Ni_3Al , NiAl : The intermetallic phase Ni_3Al is the well known γ' phase which is as coherent fcc precipitate responsible for the good creep properties of nickel base superalloys. Ni_3Al and NiAl were also considered for high temperature structural applications mainly in the 1990-ies. Powder metallurgical as well as melt metallurgical production were pursued. High production cost, lacking low temperature ductility and lacking microstructural stability were responsible that there was never a real break-through of these materials for structural applications.
- Iron aluminides, Fe_3Al : were considered for structural applications and for heat elements
- Titanium aluminides, TiAl , Ti_3Al , TiAl_3 : are used in some automotive applications. The fact that no nickel is present make them also attractive for nuclear applications
- Molybdenum di-silicide: (MoSi_2) can be considered as an electrically conducting ceramic with primary use in heating elements operating at temperatures above 1,500 °C in air. It is also considered as a material for very high temperature structural applications.
- Zirconium silicide: Zirconium silicide (Zr_3Si_2) has been identified as promising material for the neutron reflector in a gas cooled reactor.

Although the irradiation behaviour of TiAl has been studied already earlier [66, 67] currently no intermetallics are considered for structural applications in nuclear plant projects. However, the γ/α_2 titanium aluminides could have some advantages for high temperature applications [68, 69] and they were even discussed as cladding materials [70]. Figure 2.40 shows a phase diagram for the TiAl system. In the solid state, the titanium-aluminum alloys are arranged in either hcp structure (α -titanium) or bcc structure (β -titanium). Besides the α and β phases

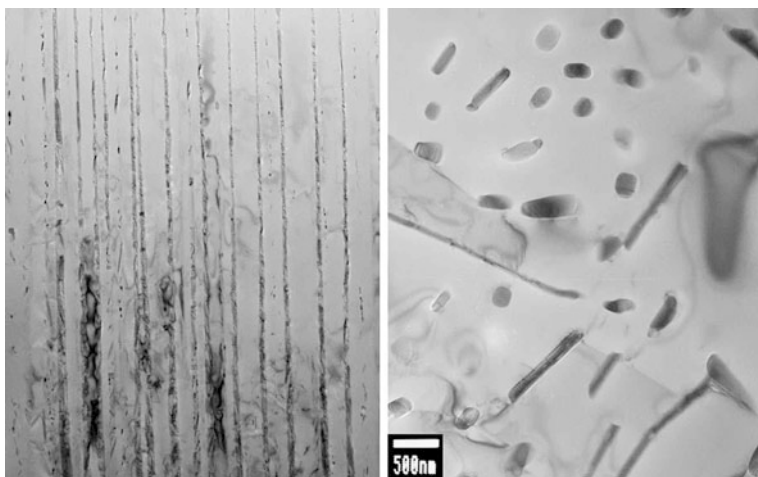


Fig. 2.41 Microstructure of a TiAl alloy. The *left* image shows the lamellar structure of γ/α_2 mixtures (γ bright), the *right* image shows equiaxed grains with islands of precipitates

there is also a Ti_3Al phase (α_2 -phase) and a γ -phase present. Both phases are of technical importance for titanium-aluminide alloys. The microstructure of a highly creep resistant γ/α_2 alloy [71] which was studied as candidate structural material for high temperature applications in advanced nuclear plants can be seen in Fig. 2.41. The two phases are mainly arranged in lamellae. Occasionally islands with globular phase morphology were found.

2.3.6 Nano-Structured Materials

Materials engineering on a nano-scale is considered as one path towards improvement of materials properties working under extreme conditions. Nano-features in structural materials described e.g. in [72–74] can improve the mechanical properties (strength, toughness etc.), surface properties (resistance against wear or corrosion) [75] or resistance against radiation damage. Besides the production of nanostructures starting from the atomic scale it is also possible to use existing normal-grained materials and process them to the required nano-structure.

Nanostructures which are important for our considerations can be grouped into the following 3 classes:

- Precipitated nano-structures
- Engineered nanostructures
- Nanostructures produced by deformation.

Precipitated nano-structures are obtained when the obstacles for dislocation movement like carbides, nitrides or any other phases can be precipitated from the

material by heat-treatment, or thermo-mechanical treatment. Guinier–Preston zones in aluminum alloys can be considered as a well-known, rather old example for such structures. In *engineered nano-structures* the obstacles are introduced from outside into the material by powder or spray techniques or other material engineering methods. Formation of nano-features under *severe plastic deformation* or thermo-mechanical treatments belong to the third class i.e. nanostructures produced by deformation. Often also combinations of these techniques are used. Particle- or cluster-strengthening is the most important application of nano-features in structural materials for nuclear energy applications. Small grains promote creep and they usually grow under thermal or irradiation conditions which limits its use for the application in advanced nuclear plants.

2.3.6.1 Oxide Dispersion Strengthening

Introduction of small ceramic particles into a metallic or intermetallic matrix for the improvement of stress rupture properties has been investigated since many years. The current (technical) state of the art was highlighted in a recent conference [76]. A very good historical perspective of the development of mechanical alloying and ODS materials can be found in [77]. The first matrices for oxide strengthening were aluminum and nickel-base superalloys. Gamma prime hardening superalloys have high melting points, excellent high temperature creep strength and very good oxidation resistance. At very high temperatures the gamma prime particles grow or dissolve and lose its strengthening capability. Ceramic dispersoids were expected to remain stable. This was the reason for the strong support that ODS-materials research received in the 70–80s of the last century particularly from the gas-turbine industry [78, 79]. At about the same time needs for improved heat-elements, heat exchanger components [80] and for fusion [81] triggered research for ferritic and martensitic ODS steels which was later joined also by the fission community with the need to improve the performance of fuel claddings for fast reactors [82, 83]. Dispersion strengthening is a classical mechanism for improving the hardness of metallic materials. It is based on the distribution (or dispersion) of only a few percent of hard, nearly insoluble particles (the dispersoids), which are non-shearable and impede plastic deformation of the matrix. Newer production experience has shown that dispersoids can partially be dissolved which will be discussed later. Dispersion strengthening is a particularly efficient means of raising the high-temperature strength and creep strength of metallic materials. A pre-requisite for this is the thermodynamic stability of the particles, which are usually chosen to be oxides. Such a dispersion can add useful strength to the matrix material even at high homologous temperatures, where other strengthening mechanisms rapidly lose their effectiveness. When applied to matrix materials such as aluminum alloys, nickel superalloys, or even intermetallic compounds, the strategy of dispersion strengthening leads to advanced materials that can be used under extreme conditions of temperature and stress. A quite good understanding of the strengthening mechanisms of ODS materials exists in the literature e.g. [85–87].

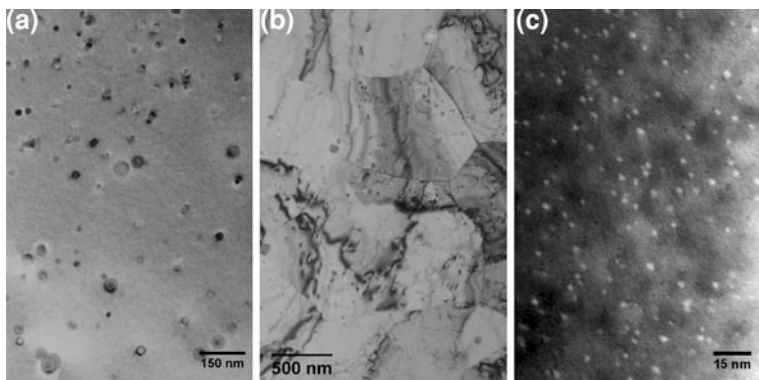


Fig. 2.42 Microstructure of different ferritic ODS materials. **a** Commercial alloy PM2000, **b** Commercial alloy PM2000 after severe plastic deformation to produce nanograins (material from G. Korb [84]), **c** Advanced ferritic 19 % Cr ODS alloy (Japanese development [83])

Dispersoids were introduced into different matrices of high temperature materials like:

- ferritic/martensitic (e.g. MA956, MA957, PM2000, 12YWT, 14YWT, \ll Super ODS \gg Japan)
- austenitic (PM1000, MA-754, MA-6000)
- intermetallics (Fe-aluminides, Ni-aluminides)
- refractory metals (Mo, W)

The main expectation for these developments was in almost all cases an increase in high temperature strength and in stress rupture properties. In case of nuclear applications also the ability of the dispersoids to act as sinks for helium became an important aspect which will be discussed later. Typical microstructures of ferritic ODS alloys are shown in Fig. 2.42. The size of the dispersoids for the advanced alloy is one order of magnitude below the one of the commercial alloy. Trials with severe plastic deformation were made which led to small grain sizes (Fig. 2.42b). This will be discussed later.

The development of ODS alloys for advanced fission reactors can be seen from Fig. 2.43 [88]. Its main driving force is the (economic) necessity to increase the burnup of the fuel. Originally, ODS steels were considered as cladding material for sodium fast reactors only operating at a maximum temperature of 550 °C. Increasing the chromium content above 16 wt. % improved strength and corrosion resistance but these alloys were prone to embrittlement. Additions of aluminum improved the corrosion resistance (aluminum oxide formation), reduced embrittlement, but also strength. Current Japanese \ll Super-ODS steels \gg contain 14–16 wt. % Cr, 4 wt. % Al, 2 wt. % W and Zr [89]. Together with the development of the chemical composition also micro- and nanostructure (grain structure, grain size, size and density of dispersoids) of the alloy could be optimized.

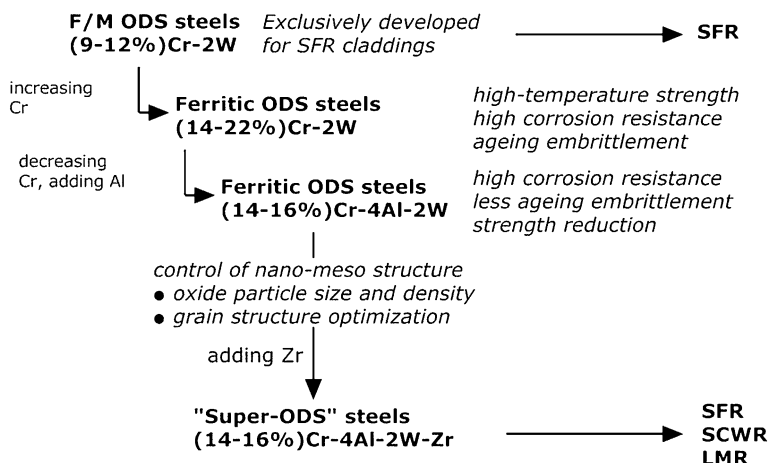


Fig. 2.43 Development path of advanced ODS cladding alloys (after [88])

The optimization of particle size and density was also triggered by the discovery that not only size and distribution of the dispersoids themselves (Y_2O_3) are of importance. Atom probe tomography studies of the commercial ODS alloy MA 957 revealed a high number density of 2–4 nm diameter nanoclusters that were enriched with Ti, Y, and O [89]. Similar observations were made with an Fe-12 wt. % Cr-3.0 % W-0.4 % Ti-0.24 % Y_2O_3 , (12YWT [90, 91]) as shown in [92] and the more recent development 14YWT [93]. These clusters were stable during long-term creep tests at 650–900 °C and they significantly reduced the creep rates [103]. Typical compositions of such alloys are Fe plus 0.2–0.5 wt. % Y_2O_3 , 0.2–1 wt. % Ti, and 1–3 wt. % W. They also contain O in excess of that introduced by the Y_2O_3 . Chromium is necessary for corrosion/oxidation resistance and tungsten is a (low-activation) solid-solution strengthener.

These ultrafine-scale features distinguish nano feature alloys (NFAs) from conventional dispersion-strengthened ODS alloys, which generally contain refined, but larger, equilibrium oxide phases. ODS alloys like PM2000 or MA956 have a high aluminum content which results in coarser features but increases the oxidation resistance which is important for high temperature applications. At the beginning of the ODS development it was primarily the thermal stability of ceramic particles forming obstacles for dislocation movement at high temperature which made ODS attractive. Generation of NFAs start from the assumption that the dispersoids are partly dissolved in the matrix during ball-milling which is the first step in currently used ODS production (see Chap. 3). Control of the milling environment supports the formation of other oxides or clusters on nano-scale. Ball milling with heavy balls creates severe plastic deformation which can consequently lead to formation of nano-grains (see also below). For an NFA with 14 %Cr (14YWT) such nano-sized grains could be obtained [93] which led at a strong Hall-Petch hardening at room temperatures. The grains remained ultrafine

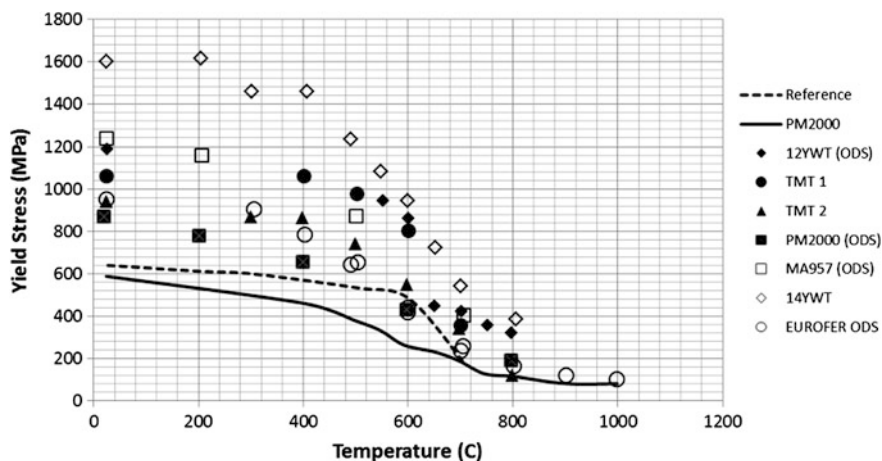


Fig. 2.44 Yield stress of different nano-particle containing steels as a function of temperature; TMT1 and TMT2 refer to different thermo-mechanical treatments. The mod. 9Cr-1Mo martensitic steel (grade 91) was taken as reference (Data from [94–98])

even after 1 h annealing at 1,000 °C [99] demonstrating the high potential of these NFAs for use under extreme conditions.

The high resistance of ferritic ODS alloys against radiation damage and its high strength make these materials also very attractive as candidates for the blanket in a fusion plant. The blanket is placed around the fusion plasma in the vacuum vessel and it is a key component of a fusion plant. Its major roles are: Extracting heat from the plasma and transferring it to the power generation system, production of fusion fuel and providing a radiation shield. Basically, the developments of ODS/NFA alloys for fusion and for fission are proceed along the same routes. However, fusion versions need to contain only low activation elements. Therefore, fusion specific alloy compositions were developed (EUROFER). The needs of high strength and radiation resistance remain the same. Figure 2.44 shows a comparison of the strength of different ODS qualities as a function of temperature.

2.3.6.2 ODS Materials Based on Non-Ferrous Matrix

The introduction of ODS versions of gamma prime hardening nickelbase superalloys into gas turbines was strongly pursued in the 1970s and 1980s. The alloys MA-754, MA-6000 and later PM1000 were considered as possible vanes and liners in advanced gas turbines [100]. Although these materials possess very good stress rupture properties at very high temperatures and good high temperature corrosion and oxidation resistance they never managed to enter into gas turbines to a significant amount [101]. ODS alloys are discussed again for gas turbines in context with engineered component design [102, 103]. In contrast to the broad R&D-effort performed to understand and improve ferritic/martensitic materials as

described above the efforts in nickel-base ODS alloys remained rather limited. Recent interest in nickelbase ODS materials (MA-754, MA-956) comes from the advanced energy applications [104] like slagging gasifiers. Although the high temperature strength of the ferritic/martensitic as well as of the nickelbase ODS alloys would be sufficient for the envisaged applications still improvements of the oxidations and corrosion resistance are considered. The fact that aluminum oxide has usually very good properties made the use of intermetallic aluminide matrices like iron-aluminides or nickel-aluminides attractive [105]. Currently, mainly R&D work is performed in this field because no clear trend for commercial applications of these intermetallics is currently visible. A comparison between ODS-Fe₃Al and ODS-FeCrAl demonstrated the formation of an alumina scale with a slow rate of oxide growth for ODS-Fe₃Al in a temperature range of 1,000–1,300 °C under isothermal conditions [106]. However, for temperatures above 1,100 °C enhanced tendency for scale spallation was reported for ODS-Fe₃Al which was attributed to a significantly higher coefficient of thermal expansion for ODS-Fe₃Al compared with FeCrAl ODS. It is speculated that the large aluminum reservoir of ODS-Fe₃Al still provides the potential for achieving greater oxidation-limited lifetimes to the ODS-FeCrAl alloys. Finally, developments towards extremely high temperatures should be mentioned. The matrix materials for this purpose are mainly refractory metals like molybdenum or tungsten (see e.g. [107, 108]). Main energy related application is the first wall in a fusion reactor. Also these developments are not entirely new. Figure 2.38 shows the very good properties of MLR which is a Lanthana reinforced molybdenum alloy.

2.3.6.3 Production of ODS and NFA

Mixing of oxides and powder in a traditional melt-metallurgical procedure is almost impossible due to powder wetting and agglomeration problems. Therefore are ODS alloys commercially produced by powder metallurgy. The process normally starts with ball milling of the metal/oxide powder mix in well defined atmospheres. The experience with NFAs described above demonstrated that the milling conditions are the key element in the production route. Consolidation can be done by hot isostatic pressing (HIP), hot extrusion or combinations of both. Afterwards the product undergoes heat treatment.

Internal oxidation would be another option for the production of ODS alloys. In this case a precursor alloy is subjected to oxidation. It was demonstrated that internal oxidation of Fe-Ti-Y and Fe-Al-Y intermetallics resulted in high volume fractions of small (~10–20 nm) oxide particles or lamellae [109]. The method is still under development but according to the literature [110] could internal oxidation become competitive with mechanical alloying in the future.

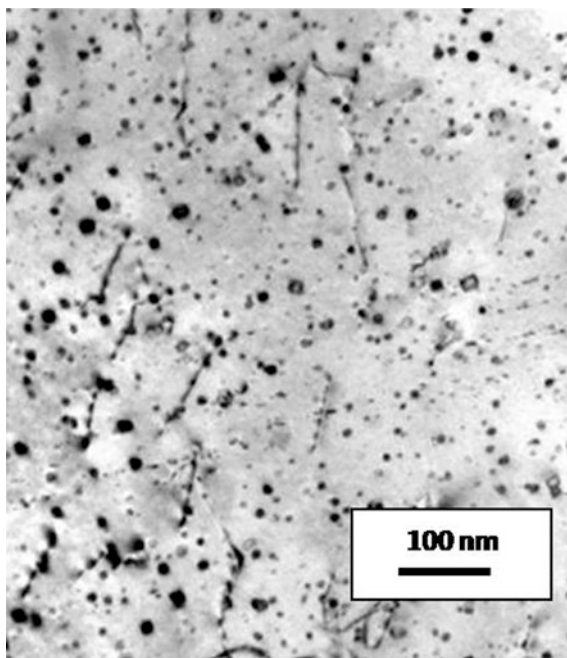
Another technique utilizes *rapid solidification through gas atomization*. These alloys are often referred to as Rapidly Solidified Powder metallurgical (RSP) materials [111]. In RSP-materials the finely dispersed particles are not only oxides,

but also nitrides and carbides. The resulting creep strength of RSP-materials typically falls in between that of conventionally produced and MA-materials [112].

Electron beam vapor deposition (EBPVD) is a candidate method for the fabrication of ODS high-temperature alloy foils. The electron beam physical vapor deposition (EBPVD) technique has superiority in its simple technical process especially for the production of large-sized foil with chosen composition and tailored microstructure [113–115]. Therefore, the fabrication of ODS high temperature alloy foils by EBPVD has attracted much attention for nickel-base ODS as well as for ferritic ODS alloys. For powder metallurgical techniques and EBPVD see also Chap. 3.

An alternative approach for the production of alloys with improved high-temperature strength is an *advanced thermo-mechanical treatment (TMT)* to obtain nano-particle strengthened martensitic steels with conventional processing techniques. The thermo-mechanical treatment consist in essence in hot-rolling plus heat treatment. While the potential improvements in properties using this approach may be somewhat more limited than those obtainable with mechanical alloying, this has the distinct advantage of being able to produce large quantities of high-temperature materials in the much nearer term. Preliminary work demonstrated the potential for significant increases in elevated temperature strength (see Fig. 2.44). Present commercial ferritic/martensitic steels are limited to maximum temperature applications in the 550–600 °C range. Initial work has demonstrated the possibilities of extending the practical temperature range for commercial steels with TMT to 650–700 °C with only limited additional processing and associated cost [116, 117]. The microstructures produced contain a very high number density of small precipitate particles (Fig. 2.45), with the result that the TMT steels show large increases in strength relative to steels produced by conventional heat treatments. Additional work is required to develop such steels for widespread service. The TMT process needs to be modified to achieve optimized strength. Understanding of the effects of the TMT processing on the microstructure and properties of these steels needs to be refined. Steels with optimized compositions for TMT need to be further developed and tested. Once the process is refined, and optimized compositions are determined, the process must be established at a commercial scale, using larger heats and TMT on appropriate geometries, such as plates or tubes. A main difference in chemical composition to conventional ferritic and ferritic-martensitic steels is the nitrogen content of the TMT steels. Nitrogen promotes the formation of nitrides or carbonitrides (MX), which can be precipitated with a diameter of a few nanometer only. According to investigations of Klueh and co-workers [118], microstructural differences between a typical martensitic steel and a TMT steel are as follows. After normalizing and tempering, commercial 9 and 12 %Cr steels have essentially a 100 % tempered martensite structure, which consists of martensite laths with a high dislocation density (10^{13} – 10^{15} m⁻²) and associated precipitates. Dominant precipitates are M₂₃C₆ particles (60–200 nm), located mainly on lath boundaries and prior-austenite grain boundaries. If vanadium and/or niobium are present,

Fig. 2.45 Small precipitations discovered in commercial 9 % Cr steel after thermomechanical treatment replotted from literature [117]



smaller (20–80 nm) MX particles form at a lower number density. Since small MX precipitates have the highest elevated temperature stability, steel with a high number density of fine MX particles should have elevated temperature properties superior to present steels. Creep strength could also be enhanced if $M_{23}C_6$ has been formed as a high density of small particles, or if the amount of larger $M_{23}C_6$ was minimized. One way to meet these conditions is to change the processing procedures of commercial steels containing nitrogen so that MX forms preferentially before $M_{23}C_6$, thus making carbon available for MX rather than $M_{23}C_6$. The effect of the TMT can be controlled by changing: austenitization temperature and time, hot-rolling temperature, amount of reduction by hot-rolling, and annealing temperature and time. Compared with the traditional powder metallurgical production the TMT process would be much simpler and therefore cheaper. The mechanical alloying process for creating oxide dispersoids is expensive and energy-intensive. Only the milling time in a high-energy ball mill for a powder is relatively long (typically 1 day). Also, mechanically alloyed materials can develop pores during high temperature annealing. TMT would be a simpler and cheaper solution. However, the expected structural applications require microstructural stability at high temperatures over long times. It has still to be demonstrated that TMT-steels have this stability and that the diameter of the nano-particles does not increase significantly.

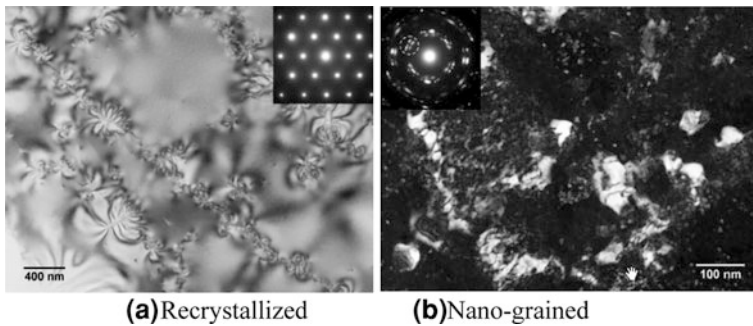


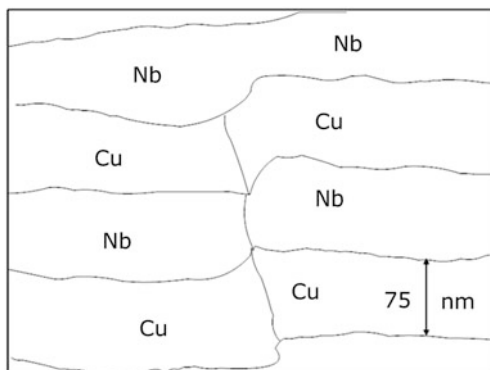
Fig. 2.46 Nano-grained Zircaloy obtained after several steps of cold rolling

2.3.6.4 Other Nano-Features

Nano-grained materials are another class of advanced materials for structural applications. Oxide dispersion strengthened materials are the most important class of nano-structured structural materials for energy applications. Production of nano-grained bulk materials is another possibility for application of nano-features. Ball milling was the earliest plastic-deformation technique for the production of nanostructured materials [119]. Powders which were treated in a ball-mill are usually only an intermediate product which needs to be further consolidated, a step which does not harm nano-sized particles but in which the nanograined structure is usually lost. For the nano-feature strengthened alloy 14YWT could be shown that extremely fine grain sizes were maintained also during consolidation [93] as already mentioned above. Nano-grains can also be obtained by massive plastic deformation of bulk materials. The most developed and significant among these techniques are equal-channel angular pressing (ECAP), high-pressure torsion (HPT), accumulative roll bonding (ARB), and surface mechanical attrition milling (SMAT) [120]. Nano-grains can be used as intermediate stage during deformation (superplastic forming) or as a microstructure possessing superior properties compared with conventional grain sizes. The high temperatures required for several applications lead usually to a significant growth of nano-grains. The fuel cladding alloys based on Zirconium (Zircaloys) can be considered as a good example. Claddings are pipes with an outer diameter of about 10 mm and a wall thickness of about 1 mm. Seamless pipes are produced according to well known procedures leading to a pronounced texture after heat treatment. To explore further development towards advanced nuclear technologies other microstructural options were considered. Zircaloy has a hcp crystallographic structure which is expected to lead to nano-grains after severe plastic deformation. A nano-grained structure could be obtained by multi-stage cold rolling [121] (Fig. 2.46) which led to an increase in strength of roughly 25 %, but after only 10 h thermal exposure at 550 °C this strength increase was lost due to grain coarsening [122].

A steel with nanometer-sized grain structure has the possibility to provide radiation resistance by increasing the grain boundary length and subsequently

Fig. 2.47 Sketch of a layered Nb/Cu nano-structure for optimized radiation resistance (original micrograph see [127])



providing a greater amount sinks for absorbing mobile defects. Optimizing the type of boundary to include a greater number of sinks might further improve the radiation resistance. The response of a 304-type austenitic material to equal channel angular pressing (ECAP) was thoroughly investigated [123], but the thermal stability was not reported. A model austenitic alloy was processed using the method for eight passes at 500 °C to obtain an average grain size of ~ 360 nm as shown in [124]. Grain boundary engineering was applied to optimize the grain boundary character distribution. Investigations of thermal stability and behaviour under irradiation are currently on track to study the properties of such austenitic steels under different service conditions. Also ferritic ODS alloys (PM2000) were ECAP-treated [84] which led to grain sizes of 500 nm and below (see Fig. 2.42). Preliminary results from tensile tests showed remarkable increase in yield stress and also in rupture elongation [125]. Due to the limited amount of data which were obtained with small tensile samples it can only be speculated that also for PM2000 an increase in yield stress and an increase in ductility can be obtained. Until which temperature and until which dpa-level the grain structure remains stable still needs to be investigated. In summary can be stated that nano-grains have a distinct potential towards improvement of properties of structural materials for nuclear applications. But this potential still needs to be further explored.

Nano-layered structures are also considered for reduction of radiation damage [126]. Collision of an energetic particle like an ion or neutron with an atom of a target creates a series of point defects (vacancies, interstitials) which can cluster before recombination leading to typical radiation damage (except helium effects). The more point defects (vacancies and interstitials) can re-combine the lower the amount which can form clusters and damage the material. Recombination may therefore be thought of as a “selfhealing” mechanism. Thus, enhancing vacancy-interstitial recombination is a strategy for improving the radiation resistance of crystalline materials. Cu-Nb multilayer composites, synthesized as thin films by magnetron sputtering with layer thicknesses ranging from 1 to several hundred nanometer are a typical example for these advanced materials (Fig. 2.47). Investigations of the stability of these structures have shown that they remained stable

up to 800 °C [127] and also under ion irradiation. Their radiation-induced defect concentrations are far below those of pure fcc Cu and bcc Nb subjected to similar dpa levels, and decrease with decreasing thickness of the individual layers, demonstrating the capability of self-healing of radiation damage. Traditionally, materials development starts at existing materials grounds from which further improvements are developed by materials optimization. Changes in chemical composition, heat treatment or—as discussed before—the introduction of new strengthening elements are typical examples for this type of development. Atomic-scale design aims to achieve superior radiation response by purposefully manipulating composition and microstructure to control the behavior of radiation-induced defects. Currently materials modeling is a means to determine the impact of modifications on materials behaviour and/or to accelerate improvement of existing materials. In (farer) future modeling could help to realize unconventional materials that could not have arisen through a series of gradual modifications. Radiation damage happens on an atomic scale and it is therefore well suited for demonstration of the capabilities of materials modeling for the development of new structures which are tailored to certain properties [126, 128].

2.3.7 Ceramic Materials

Graphite, oxide ceramics and carbide ceramics are considered as structural materials for advanced nuclear plants. Currently, only a few candidates are really investigated: Graphite and SiC compounds are of highest interest.

2.3.7.1 Graphite

Properties of graphite for nuclear applications were described extensively in the literature like e.g. [129, 130].

Graphite in nuclear plants can have two functions: It acts as a moderator by slowing down fast neutrons and it is responsible for the structural stability of core components made out of graphite. It is a key structural element in gas cooled reactors using a thermal neutron spectrum (AGR, HTR). The structural integrity must be retained over a wide range of neutron fluence and reactor temperatures. In the British AGRs commercial graphite moderator systems have run for over forty years. Nuclear graphites were also successfully used in earlier HTR-projects. A large database for graphite exists but there are still uncertainties concerning details of graphite production. Some details might have disappeared over the years because of the declining interest in HTRs until recently. Graphite is produced synthetically in large blocks. In the absence of both air and neutron irradiation, at temperatures up to about 2,000 °C, structural integrity is maintained.

Graphite is very different from the metallic materials used in current and future nuclear plants. In contrast to an alloy which has high strength, ductility, no

Table 2.7 Important characteristics of graphite, wg... with grain, ag... against grain (*source* [129])

Property	Steel alloy 316L	Specialty extruded graphite
Density (g/cm ³)	8.0 (Porosity = 0 %)	1.74 (Porosity = 23 %)
Tensile, MPa	>480	15/11 wg/ag
Elongation at break	>40	0.3
Poisson’s ratio	0.3	0.2
Thermal conductivity, W/mK	17	160/145 wg/ag
Thermal expansion (CTE) 10 ^{−6} K ^{−1}	18	2.5/3.6 wg/ag

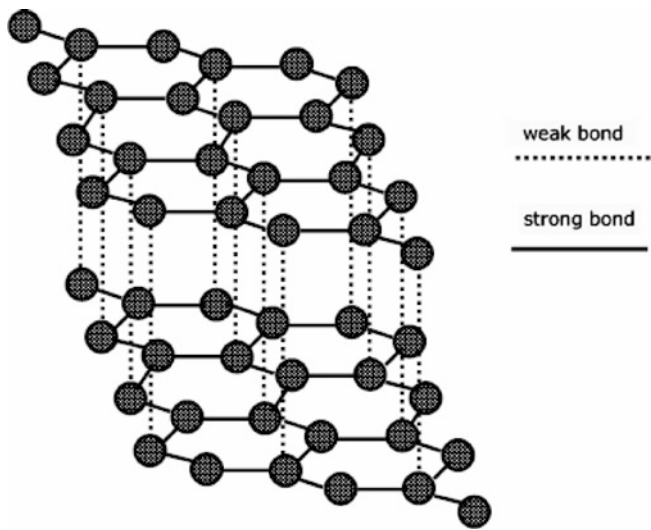
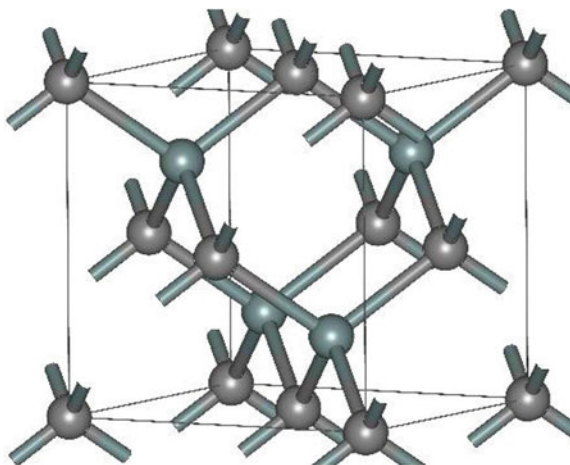


Fig. 2.48 Crystal lattice of graphite

porosity and homogeneity, bulk graphite has low strength and is brittle, porous and inhomogeneous. Some of the differences between graphite and the austenitic steel 316L as a typical alloy for nuclear applications, are listed in Table 2.7 together with important properties of bulk graphite [129]. Graphite has several advantages: it is chemically inert, does not show phase changes and it allows a wide variation in properties without change in chemical composition. Strength improves for temperatures up to 2,000 °C (provided oxidizing gases are excluded) and graphite has a high resistance to thermal shock. Its ability to slow down (moderate) fast neutrons is the most important property with respect to nuclear applications. A distinct characteristic of graphite is its anisotropy. This anisotropy is reflected in its microstructure shown in Fig. 2.48. Graphite consists of planes with hexagonal atom arrangement which are weakly bonded. This anisotropy has an important influence on the behaviour of graphite under irradiation as shown in Chap. 5. The anisotropy can also be seen from properties given in Table 2.7 where the notations

Fig. 2.49 Structure of β -SiC which is the preferred structure for fiber reinforced SiC [131]

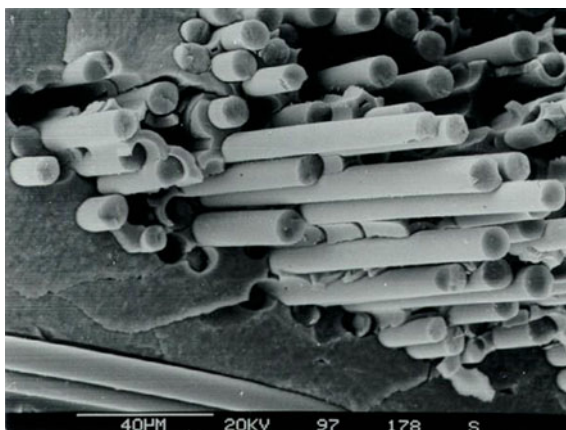


wg (with grain) and ag (against grain) are introduced. With-grain means parallel to the extrusion direction and against-grain means perpendicular to the extrusion direction. The anisotropy, usually observed in graphite products, is also established in the forming operation. In extruded products, the anisotropic coke particles orient with their long dimensions parallel to the extrusion direction. Proper particle size, geometry and distribution are therefore extremely important for the properties of the final product which should be near-isotropic. But also coke type, particle size, and the ratio of die-to-mold chamber diameters have a strong influence on isotropy of the final product.

2.3.7.2 Silicon Carbide

Bulk Silicon Carbide is the only chemical compound of carbon and silicon. It was originally produced by a high temperature electro-chemical reaction of sand and carbon. Silicon carbide is an excellent abrasive and has been produced and made into grinding wheels and other abrasive products for over one hundred years. The material can also be made an electrical conductor and has applications in resistance heating, flame igniters and electronic components. Silicon carbide has also attractive strength properties at temperatures up to 1,600 °C and it has therefore been considered since many years as a possible structural material for high temperature applications. The main obstacle is its low fracture toughness making several components extremely prone to brittle fracture. It is a candidate for fusion (mainly tiles) and for fission (as layered structure in HTR fuel). Silicon carbide is composed of tetrahedra of carbon and silicon atoms with strong bonds in the crystal lattice. This produces a very hard and strong material. Silicon carbide is not attacked by any acids or alkalis or molten salts up to 800 °C. In air, SiC forms a protective silicon oxide coating at 1,200 °C and is able to be used with almost no strength loss up to 1,600 °C. Silicon carbide exists in about 250 crystalline forms.

Fig. 2.50 Microstructure of a SiC/SiC compound [134]



The polymorphism of SiC is characterized by a large family of similar crystalline structures called polytypes. They are variations of the same chemical compound that are identical in two dimensions and differ in the third. Thus, they can be viewed as layers stacked in a certain sequence [132]. Beta SiC (Fig. 2.49) is the modification of the matrix of many fiber reinforced SiCs discussed for nuclear applications.

Nano-crystalline SiC is currently studied to further improve mechanical properties like toughness [133] and it might also have superior radiation damage resistance. Bulk SiC is rather brittle and it can therefore only be used as structural material. It is e.g. employed in highly corrosive environments of the iodine sulfur process for thermo-chemical hydrogen production.

Silicon carbide (SiC) composites belong to the class of ceramic fiber reinforced ceramics (CFC). They consist of a woven fiber structure (in our case silicon carbide or carbon) which is embedded into a ceramic matrix (in our case SiC) as shown in Fig. 2.50 [134]. The fibers prevent brittle fracture of the SiC-matrix (see Chap. 4) and make the material suitable for structural applications. Currently only limited structural applications (tiles for aerospace applications, brakes, hot gas liners etc.) exist. One of the main current obstacles is the price for components. SiC/SiC is a candidate material for low-activation structural applications in proposed fusion reactors. It is also considered for advanced fission reactors for applications like VHTR control rod, GFR cladding, MSR claddings and/or structural components. Fiber reinforced ceramics are engineered materials which need a very good tuning between matrix, fiber and fiber matrix interface. The bulk of work done with respect to nuclear applications comes from the fusion materials society. Much work has been done for the development of fibers and fiber surfaces to obtain the required radiation resistance. For cladding applications it is most important that the material remains gas tight under reactor operation conditions which is currently investigated for advanced reactors [135] and (particularly after the Fukushima event also for LWRs.

2.3.8 Coatings

The increasing demands in advanced nuclear applications (temperature, corrosive environment) can most probably only be accommodated with surface protection. Coatings can be applied to protect against hot corrosion, erosion and wear and they can also be employed as thermal barriers. Although coating technology is well accepted in non-nuclear machinery it is new in the field of nuclear applications. Conditions in advanced liquid metal reactors (operating at temperatures above 550 °C) and in molten salt reactors will probably need alumina formers for surface protection. Many coatings are designed to be consumed with time (aluminum or chromium donors) and also coatings are not considered as a design issue. This means that the whole safety and reliability culture for coatings has to be built up for future reactors. Current coating trials for fission reactors are primarily based on existing compositions which were mainly developed for gas turbines. Developments towards nano-powders or nano-composites might help to improve quality and life-time of coatings in future. More about application of coatings can be found in [Chap. 3](#).

References

1. Guzonas D (2009) SCWR materials and chemistry status of ongoing research. In: GIF symposium—Paris (France), 9–10 Sept 2009, pp 163–171
2. Buckthorpe D, Heikinheimo L, Fazio C, Hoffelner W, van der Laan JG, Nilsson KF, Schuster F (2012) Scientific assessment in support of the materials roadmap enabling low carbon energy technologies-technology nuclear energy. http://setis.ec.europa.eu/activities/materialsroadmap/Scientific_Assessment_NuclearEnergy. Accessed 3 July 2012
3. Nabarro FRN, Hirth JP (eds) (2009) Dislocations in Solids, Series, vol 16. Elsevier, Amsterdam
4. Haasen P, Mordike BL (1996) Physical metallurgy, 3rd edn. Cambridge University Press, Cambridge
5. Hull D, Bacon DJ (2001) Introduction to dislocations, 4th edn. Butterworth and Heinemann, London
6. Frank-Read source, http://en.wikipedia.org/wiki/Frank-Read_Source. Accessed 15 Sept 2011
7. Seeger A (1957) Dislocations and mechanical properties of crystals. Wiley, New York
8. Schäublin R, Yao Z, Baluc N, Victoria M (2005) Irradiation-induced stacking fault tetrahedra in fcc metals. *Phil Mag* 85:769–777
9. Kadoyoshi T, Kaburaki H, Shimizu F, Kimizuka H, Jitsukawa S, Lie J (2007) Molecular dynamics study on the formation of stacking fault tetrahedra and unfaulting of Frank loops in fcc metals. *Acta Mater* 55:3073–3080
10. Smigelskas AD, Kirkendall EO (1947) Zinc diffusion in alpha brass. *Trans AIME* 171: 130–142
11. ASM Handbook of Alloy Phase Diagrams (1992) ASM International, Cleveland ISBN: 978-0-87170-381-1
12. University of Cambridge: DoITPoMS teaching and learning packages <http://www.doitpoms.ac.uk/tlplib/phase-diagrams/intro.php>. Accessed 8 Oct 2011

13. Porter DA, Easterling K (1992) Phase transformations in metals and alloys, 2nd edn. Routledge, London
14. Smallman RE (1985) Modern physical metallurgy. Butterworth, London
15. John V (1974) Understanding phase diagrams. Macmillan, New York
16. Allen TR, Busby JT, Klueh RL, Maloy SA, Toloczko MB (2008) Cladding and duct materials for advanced nuclear recycle reactors. *J Mater* 60(1):15–25
17. Strassland JL, Powell RW, Chin BA (1982) An overview of neutron irradiation effects in LMFBR materials. *J Nucl Mater* 108–109:299
18. Zinkle S (2008) In: Structural materials for innovative nuclear systems (SMINS) Workshop proceedings Karlsruhe, Germany, 4–6 June 2007 SMINS NEA no. 6260
19. Iron-Carbon Phase Diagram. <http://www.calphad.com/iron-carbon.html>
20. Wikipedia <http://en.wikipedia.org/wiki/Pearlite>. Accessed 8 Oct 2011
21. Llewellyn DT, Hudd RC (1998) Steels: metallurgy and applications. Butterworth-Heinemann, London
22. Schaeffler AL (1949) Constitution diagram for stainless steel weld metal. In: Metal progress. American Society for Metals Cleveland Ohio, vol 56, pp 680–680B. ISSN 0026-0665
23. The Schaeffler and Delong diagrams for predicting ferrite levels in austenitic stainless steel welds. <http://www.bssa.org.uk/topics.php?article=121>. Accessed 8 Oct 2011
24. Transformation diagrams (CCT and TTT). http://www.matter.org.uk/steelmatter/metallurgy/7_1_2.html. Accessed 8 Oct 2011
25. Reference manual on the IAEA JRQ correlation monitor steel for irradiation damage studies (2001) IAEA-TECDOC-1230
26. http://www.spaceflight.esa.int/impress/text/education/Glossary/Glossary_P.html. Accessed 8 Oct 2011
27. <http://www.msm.cam.ac.uk/phase-trans/abstracts/chang.html>. Accessed 8 Oct 2011
28. <http://www.threeplanes.net/martensite.html>. Accessed 8 Oct 2011
29. Buckthorpe D (2002) https://odin.jrc.ec.europa.eu/htr-tn/HTR-Eurocourse-2002/Buckthorpe_582.pdf. Accessed 8 Oct 2011
30. Klueh RL (2004) Elevated-temperature ferritic and martensitic steels and their application to future nuclear reactors. ORNL/TM-2004/176
31. Klueh RL, Harries DR (2001) High-chromium ferritic and martensitic steels for nuclear applications ASTM STP MONO3
32. Masuyama F (1999) In: Viswanathan R, Nutting J (eds) Advanced Heat Resistant Steel for Power Generation. The Institute of Materials, London, pp 33–48
33. Viswanathan R, Bakker W (2001) Materials for ultrasupercritical coal power plants—boiler materials. *J Mater Eng Perf* 10:81–95
34. Viswanathan R, Bakker W (2001) Materials for ultrasupercritical coal power plants, Part 2. *J Mater Eng Perf* 10:96–101
35. Ryu WS, Kim SH (2010) Thermal treatment improving creep properties of nitrogen-added Mod.9Cr-1Mo steels. *Trans Indian Inst Met* 63(2–3):39–43
36. Lindau R, Möslang A, Rieth M, Klimiankou M, Materna-Morris E, Alamo A, Tavassoli AAF, Cayron C, Lancha AM, Fernandez P, Baluc N, Schäublin R, Diegele E, Filacchioni G, Rensman JW, v.d. Schaaf B, Lucon E, Dietz W (2005) Present development status of EUROFER and ODS-EUROFER for application in blanket concepts. *Fusion Eng Des* 75–79: 989–996
37. Ehrlich K, Cierjacks SW, Kelzenberg S, Möslang A (1996) The development of structural materials for reduced long-term activation. ASTM Special Technical Publications, STP 1270:1109–1122
38. van der Schaaf B, Tavassoli F, Fazio C, Rigal E, Diegele E, Lindau R, LeMarois G (2003) The development of EUROFER reduced activation steel. *Fusion Eng Des* 69(1–4):197–203
39. Klueh RL, Maziasz PJ, Alexander DJ (1996) Bainitic chromium-tungsten steels with 3 Pct chromium. *Metall Mater Trans A* 28(2):335–345. doi:10.1007/s11661-997-0136-0
40. Scott X, Mao SX, Vinod K, Sikka VK (2006) Fracture toughness and strength in a new class of bainitic chromium-tungsten steels. Oak Ridge National Laboratory. ORNL/TM-2006/44

41. Stainless steels—introduction to the grades and families <http://www.azom.com/article.aspx?ArticleID=470>. Accessed 8 Oct 2011
42. Raj B, Mannan SL, Vasudeva PR, Rao K, Mathew MD (2002) Development of fuels and structural materials for fast breeder reactors. *Sadhana* 27(5):527–558
43. Latha S, Mathew MD, Bhanu Sankara Rao K, Mannan SL (2001) Creep properties of 15Cr-15Ni austenitic stainless steel and the influence of titanium. In: Parker J (ed) *Creep and fracture of engineering materials and structures*. The Institute of Materials, London, pp 507–513
44. Microstructures in Austenitic Stainless Steels, key-to-metals, Article, <http://www.keytometals.com/page.aspx?ID=CheckArticle&site=kts&NM=268>. Accessed 13 Oct 2011
45. Guy K, Cutler EP, West DRF (1982) Epsilon and alpha' martensite formation and reversion in austenitic stainless steels. *J de Physique Colloque C4 supplement no 12 43 C4-575-580*
46. Kalkhof D, Grosse M, Niffenegger M, Leber HJ (2004) Monitoring fatigue degradation in austenitic stainless steels. *Fatigue Fract Eng Mater Struct* 27(7):595–607
47. Fahr D (1973) Analysis of stress-strain behaviour of type 316 stainless steel. ORNL TM 4292
48. Wang J, Zou H, Li C, Peng Y, Qiu S, Shen B (2006) The microstructure evolution of type 17- 4PH stainless steel during long-term aging at 350 °C. *Nucl Eng Des* 236:2531–2536
49. Viswanathan UK, Banerjee S, Krishnan U (1988) Effects of aging on the microstructure of 17-4 PH stainless steel. *Mater Sci Eng A* 104:181–189
50. Superalloys: a primer and history, TMS (2000) <http://www.tms.org/meetings/specialty/superalloys2000/superalloyshistory.html>. Accessed 13 Oct 2011
51. Nickel-based superalloys: part one, article <http://www.keytometals.com/page.aspx?ID=CheckArticle&site=ktn&LN=FR&NM=234>. Accessed 8 Oct 2011
52. Sims CT, Stoloff NS, Hagel WC (1987) *Superalloys II*, 1st edn. ISBN-10: 0-471-01147-9 ISBN-13: 978-0-471-01147-7. Wiley, New York
53. Donachie MJ, Donachie SJ (2002) *Superalloys a technical guide*, ASM International, Cleveland
54. Special metals, the story of the INCOLOY alloys series from 800 through 800H 800HT. <http://www.specialmetals.com/documents/Incoloy%20alloys%20800H%20800HT.pdf>. Accessed 8 Oct 2011
55. Special metals, data sheet, <http://www.specialmetals.com/documents/Inconel%20alloy%20600%20%28Sept%202008%29.pdf>. Accessed 8 Oct 2011
56. Special metals datasheet, <http://www.specialmetals.com/documents/Inconel%20alloy%20617.pdf>. Accessed 8 Oct 2011
57. Wright JK, Carroll LJ, Cabot CJ, Lillo T, Benz JK, Simpson JA, Lloyd WR, Chapman JA, Wright RN (2010) Characterization of elevated temperature properties of heat exchanger and steam generator alloys. In: *Proceedings of HTR 2010 Prague Czech Republic*, p 31, 18–20 Oct 2010
58. Ren W, Swindeman R (2009) A review on current status of alloys 617 and 230 for Gen IV nuclear reactor internals and heat exchangers. *Trans ASME* 131:044002–044017
59. Wu Q, Song H, Swindeman RW, Shingledecker JP, Vijay K, Vasudevan VK (2008) Microstructure of long-term aged IN617 Ni-base superalloy. *Met Mat Trans A* 39A:2569
60. HA-230 Datasheet Haynes <http://www.haynesintl.com/230HaynesAlloy.htm>. Accessed 18 Oct 2011
61. Kondo T development and testing of alloys for primary circout structures of a VHTR, IAEA knowledge base. http://www.iaea.org/inisnkm/nkm/aws/htrg/fulltext/iwggcr4_3.pdf, visited July 2011
62. Hastelloy N (2002) Datasheet, Haynes International, Inc. H-2052B <http://www.haynesintl.com/pdf/h2052.pdf>. Accessed 19 Oct 2011
63. Murty KL, Charit I (2008) Structural materials for Gen-IV nuclear reactors: challenges and opportunities. *J Nucl Mater* 383:189–195
64. Knabl W, Schulmeyer W, Stickler R (2010) Plansee refractory metals: properties, applications and industrial fabrication, workshop: Innovative Materials Immune To Radiation (IMIR). <http://www.engconfintl.org/10akpapers.html>. Accessed 19 Oct 2010

65. Romero J, Quinta da Fonseca J, Preuss M, Dahlbäck M, Hallstadius L, Comstock R (2010) Texture evolution of zircaloy-2 during beta quenching: effect of process variables ASTM, Technical Committees/Committee B10 on Reactive and Refractory Metals and Alloys. http://www.astm.org/COMMIT/B10_Zirc_Presentations/index.html. Accessed 19 Oct 2011
66. Hishinuma A, Fukai K, Sawai T, Nakata K (1996) Ductilization of TiAl intermetallic alloys by neutron-irradiation. *Intermetallics* 4(3):179–184. doi:10.1016/0966-9795(95)00030-5
67. Hishinuma A (1996) Radiation damage of TiAl intermetallic alloys. *J Nucl Mater* 239: 267–272. doi:10.1016/S0022-3115(96)00429-1
68. Magnusson P, Chen J, Höffelner W (2009) Thermal and irradiation creep behavior of a titanium aluminide in advanced nuclear plant environments. *Met Mat Trans A* 40A:2837–2842. doi:10.1007/s11661-009-0047-3
69. Magnusson P (2011) Thermal and irradiation creep of TiAl. Doctoral Thesis. EPFL Lausanne and Paul Scherrer Institute Switzerland
70. Kim YW, Kim SL, Woodward C (2010) Gamma (TiAl) alloys: breaking processing and grain size barriers. IMIR-1 2010 0822-0826 Vail CO
71. Lapin J, Nazmy M (2004) Microstructure and creep properties of a cast intermetallic Ti-46Al-2 W-0.5Si alloy for gas turbine applications. *Mater Sci Eng A* 380:298–307
72. Gleiter H (2000) Nanostructured materials: basic concepts and microstructure. *Acta Mater* 48:1–29
73. Weertman JR (2007) Mechanical behavior of nanocrystalline metals. In: Koch CC (ed) *Nanostructured materials: processing properties and applications*, 2nd edn. William Andrew Inc, New York, pp 537–564
74. Gell M (1995) Application opportunities for nanostructured materials and coatings. *Mater Sci Eng A* 204:246–251
75. Koch CC (ed) *Nanostructured materials: processing properties and applications*, 2nd edn. William Andrew Inc, New York, pp 91–118
76. ODS (2010) Materials workshop. In: Conference Proceedings Qualcomm Conference Ctr Jacobs Hall UCSD La Jolla CA Nov 17–18th <http://structures.ucsd.edu/ODS2010/>. Accessed 19 Oct 2011
77. Jones A (2010) Historical perspective: ods alloy development. See [76] Enduser Perspectives
78. Benn RC, Kang SK (1984) In: Gell M et al. (eds) *Proceedings Conference Superalloys*. TMS-AIME, pp 319
79. Ewing BA, Jain SK (1988) Development of inconel alloy MA 6000 turbine blades for advanced gas turbine engine designs. In: Duhl DN, Maurer G, Antolovich S, Lund C, Reichman S (eds) *Superalloys 1988 TMS*, pp 131–140
80. Starr F (2010) The ODS alloy high temperature heat exchanger and associated work. See [76] Enduser Perspectives
81. Oksiuta Z, Olier P, de Carlan Y, Baluc N (2009) Development and characterisation of a new ODS ferritic steel for fusion reactor applications. *J Nucl Mater* 393(1):114–119
82. Kimura A, Ukai S, Fujiwara M (2004) R&D of oxide dispersion strengthening steels for high burn-up fuel claddings. In: *Proceedings of International Congress Advances in Nuclear Power Plants (ICAPP-2004)* ISBN 0-89448-680-2, pp 2070–2076
83. Kimura A, Cho HS, Toda N, Kasada R, Yutani K, Kishimoto H, Iwata N, Ukai S, Fujiwara M (2008) High Cr-ODS steels R&D for high burn-up fuel claddings. In: *Structural materials for innovative nuclear systems (SMINS) Workshop Proceedings Karlsruhe*. Germany 4–6 June 2007 NEA No 6260 OECD, pp 103–114
84. Korb G (2008) Research Center Seibersdorf (Austria,) EU FW6 project EXTREMAT
85. Arzt E (1991) Creep of dispersion strengthened materials: a critical assessment. *Res Mechanica* 31:399–453
86. Blum W, Reppich B (1985) Creep of particle-strengthened alloys. In: Wilshire B, Evans RW (eds) *Creep behavior of crystalline solids*. Pineridge Press Swansea UK, pp 83–136
87. Rösler J (2003) Particle strengthened alloys for high temperature applications: strengthening mechanisms and fundamentals of design. *J Mater Prod Technol* 18(1–3):70–90

88. Kimura A, Kasada R, Iwata N, Kishimoto H, Zhang CH, Isselin J, Dou P, Lee JH, Muthukumar N, Okuda T, Inoue M, Ukai S, Ohnuki S, Fujisawa T, Abe TF (2010) Super ODS steels R&D for fuel cladding of Gen-IV systems, Innovative Materials Immune to Radiation (IMIR)-1, 22–26 Aug 2010 The Lodge at Vail CO
89. Miller KM, Hoelzer DT, Kenik EA, Russell KF (2004) Nanometer scale precipitation in ferritic MA/ODS alloy MA957. *J Nucl Mater* 329–333:338–341
90. Ukai S, Nishida T, Okada H, Okuda T, Fujiwara M, Asabe K (1997) Development of oxide dispersion strengthened ferritic steels for fbr core application (I) improvement of mechanical properties by recrystallization processing. *J Nucl Sci Technol* 34(3):256
91. Ukai S, Nishida T, Okuda T, Yoshitake T (1998) Development of oxide dispersion strengthened ferritic steels for fbr core application (II) morphology improvement by martensite transformation. *J Nucl Sci Technol* 35(4):294
92. Miller MK, Hoelzer DT, Babu SS, Kenik EA, Russell KF (2003) High temperature microstructural stability of a MA/ODS ferritic alloys. In: Fuchs GE, Wahl JB (eds) High temperature alloys: processing for properties. The Minerals Metals and Materials Society
93. Hoelzer DT, Bentley J, Miller MK, Sokolov MK, Byun TS, Li M (2010) Development of high-strength ODS steels for nuclear energy applications. In: ODS 2010 materials workshop qualcomm conference center Jacobs Hall University of California, San Diego, 17–18 Nov 2010
94. Hoffelner W (2010) Development and application of nano-structured materials in nuclear power plants. In: Tipping PG (ed) Understanding and mitigating ageing in nuclear power plants. Woodhead, pp 581–605
95. Klueh RL, Hashimoto N, Maziasz PJ (2005) Development of new ferritic/martensitic steels for fusion applications. In: Fusion engineering 2005 twenty-first IEEE/NPS symposium on fusion materials, pp 1–4. <http://ieeexplore.ieee.org/stamp/stamp.jsp?arnumber=4018942&isnumber=401887>. Accessed 20 Oct 2011
96. Alamo A, Lambard V, Averty X, Mathon MH (2004) Assessment of ODS-14%Cr ferritic alloy for high temperature applications. *J Nucl Mater Part 1*:333–337
97. Klueh RL, Shingledecker JP, Swindeman RW, Hoelzer DT (2005) Oxide dispersion-strengthened steels: a comparison of some commercial and experimental alloys. *J Nucl Mater* 341:103–114
98. Byun TS, Hoelzer DT, Kim JH (2010) High Temperature Fracture Characteristics of Nanostructured Ferritic Alloy. In: Innovate materials immune to radiation 22–26 Aug 2010, Vail CO USA IMIR-1
99. Schneibel JH, Liu CT, Miller MK, Mills MJ, Sarosi P, Heilmaier M, Sturm D (2009) Ultrafine-grained nanocluster-strengthened alloys with unusually high creep strength. *Scripta Mater* 61:793–796
100. Benn RC, McColvin GM (1988) The development of ODS superalloys for industrial gas turbines. In: Reichman S, Duhl DN, Maurer G, Antolovich S, Lund C (eds) Superalloys 1988, The metallurgical society, pp 73
101. Donachie MJ, Donachie SJ (2002) Superalloys: a technical guide, 2nd edn, ASM, Cleveland
102. James A (2010) The challenge for ODS materials: an industrial gas turbine perspective, see [76]
103. Kang B, Ogawa K, Ma L, Alvin MA, Wu N, Smith G (2009) Materials and component development for advanced turbine systems—ODS alloy development. In: 23rd annual conference on fossil energy materials Pittsburgh, 12–14 May 2009
104. Hurley JP (2010) ODS Alloys in coal-fired heat exchangers—prototypes and testing, 2010 ODS Alloy workshop San Diego California, 17–18 Nov 2010. See also [76]
105. Kad BK, Wright I, Smith G, Judkins R (2003) Optimization of oxide dispersion strengthened alloy tubes. <http://www.ms.ornl.gov/fossil/pdf/Subcontract/UCSD-Topical-2003.pdf>. Accessed 20 Oct 2011
106. Chevalier S, Juzon P, Borchardt G, Galerie A, Przybylski K, Larpin JP (2010) High-temperature oxidation of Fe3Al and Fe3Al–Zr intermetallics. *Oxid Met* 73:43–64. doi:10.1007/s11085-009-9168-8

107. Poerschke DL (2009) Mechanical properties of oxide dispersion strengthened molybdenum alloys. Department of Materials Science and Engineering Case Western Reserve University
108. Mueller AJ, Shields JA, Buckman RW (1999) The effect of thermo-mechanical processing on the mechanical properties of molybdenum—2 vol% Lanthana Bettis Atomic Power Lab DE-AC11-98PN38206
109. Schneibel JH, Kad BK Nanoprecipitates in steels. <http://www.pdfbe.com/8e/8e628cc0c308f5f0-download.pdf>. Accessed 20 Oct 2011
110. Schneibel JH, Shim S (2008) Nano-scale oxide dispersoids by internal oxidation of Fe–Ti–Y intermetallics. *Mater Sci Eng A* 488:134–138
111. Rieken JR, Anderson IE, Kramer MJ, Wu YQ, Anderegg JW, Kracher A, Besser MF (2008) Atomized precursor alloy powder for oxide dispersion-strengthened ferritic stainless steel. In: *Advances in powder metallurgy and particulate materials*. MPIF, Washington
112. Jönsson B, Berglund R, Magnusson J, Henning P, Hättestrand M (2004) High temperature properties of a new powder metallurgical FeCrAl alloy. *Mater Sci Forum* 461–464:455–462
113. Srinivasan D, Corderman R, Subramanian PR (2006) Strengthening mechanisms (via hardness analysis) in nanocrystalline NiCr with nanoscaled Y_2O_3 and Al_2O_3 dispersoids. *Mater Sci Eng A* 416:211
114. Chen S, Qu SJ, Han JC (2009) Microstructure and mechanical properties of Ni-based superalloy foil with nanocrystalline surface layer produced by EB-PVD. *J Alloy Compd* 484:626
115. Lin X, He X, Sun Y, Li Y, Guangping Song G, Xinyan Li X, Jiazhen Zhang J (2010) Morphology and texture evolution of FeCrAlTi– Y_2O_3 foil fabricated by EBPVD. *Surf Coat Technol* 205:76–84
116. Klueh RL, Hashimoto N, Maziasz PJ (2007) New nano-particle-strengthened ferritic/martensitic steels by conventional thermo-mechanical treatment. *J Nucl Mater* 367–370(1): 48–53
117. Klueh RL, Hashimoto N, Maziasz PJ (2005) Development of new nano-particle-strengthened martensitic steels. *Scripta Mater* 53:275–280
118. Klueh RL (2010) Toward new high-temperature ferritic/martensitic steels. IMIR Workshop Vail CO, 26 Aug 2010
119. Zhu Y, Valiev RZ, Langdon TG, Tsuji N, Lu K (2010) Processing of nanostructured metals and alloys via plastic deformation. *MRS Bulletin* vol 35:977–981
120. Misra A, Thilly L (2010) Structural materials at extremes. *MRS Bull* 35:965–972
121. Hoffelner W, Froideval A, Pouchon M, Chen J, Samaras M (2008) Synchrotron X-Rays for microstructural investigations of advanced reactor materials. *Met Mat Trans A* 39:214
122. Chen J, Hoffelner W, Rebac T (2010) Paul Scherrer Institut, Switzerland. Unpublished
123. Huang CX, Yang G, Deng B, Wu SD, Li SX, Zhang ZF (2007) Formation mechanism of nanostructures in austenitic stainless steel during equal channel angular pressing. *Phil Mag* 87(31):4949–4971
124. Yang Y, Ch. Sun C, X. Zhang X, A. Todd (2011) Effect of grain size and grain boundaries on the proton irradiation response of nanostructured austenitic model alloy. TMS Annual Meeting. *Microstructural Processes in Irradiated Materials* TMS
125. Froideval A, Chen J, Pouchon M, Hoffelner W (2011) Paul Scherrer Institut, Switzerland. Unpublished
126. Demkowicz MJ, Bellon P, Wirth BD (2010) Atomic-scale design of radiation-tolerant nanocomposites. *MRS Bull* 35:992–998
127. Misra A, Hoagland RG, Kung H (2004) Thermal stability of self-supported nanolayered Cu/Nb films. *Phil Mag* 84(10):1021–1028
128. Demkowicz MJ, Hoagland RG, Hirth JP (2008) Interface structure and radiation damage resistance in Cu–Nb multilayer nanocomposites. *Phys Rev Lett* 100:136102
129. Ball DR (2008) Graphite for high temperature gas-cooled nuclear reactors. ASME LIC STP-NU-009
130. Turk DL (2000) Graphite, processing artificial Kirk-Othmer encyclopedia of chemical technology. Wiley, New York, Published Online: 4 Dec 2000

131. Silicon Carbide. Wikipedia http://en.wikipedia.org/wiki/Silicon_carbide. Accessed 8 Oct 2011
132. Properties of Silicon Carbide (SiC). Ioffe Institute. <http://www.ioffe.ru/SVA/NSM/Semicond/SiC/>. Accessed 18 Oct 2011
133. Szlufarska I, Nakano A, Vashishta P (2005) A crossover in the mechanical response of nanocrystalline ceramics. *Science* 309:911
134. MT Aerospace, http://de.wikipedia.org/wiki/Keramischer_Faserverbundwerkstoff
135. Katoh Y, Cozzi A (eds) (2010) *Ceramics in nuclear applications*. Wiley, New York

<http://www.springer.com/978-1-4471-2914-1>

Materials for Nuclear Plants

From Safe Design to Residual Life Assessments

Hoffelner, W.

2013, XXX, 482 p., Hardcover

ISBN: 978-1-4471-2914-1